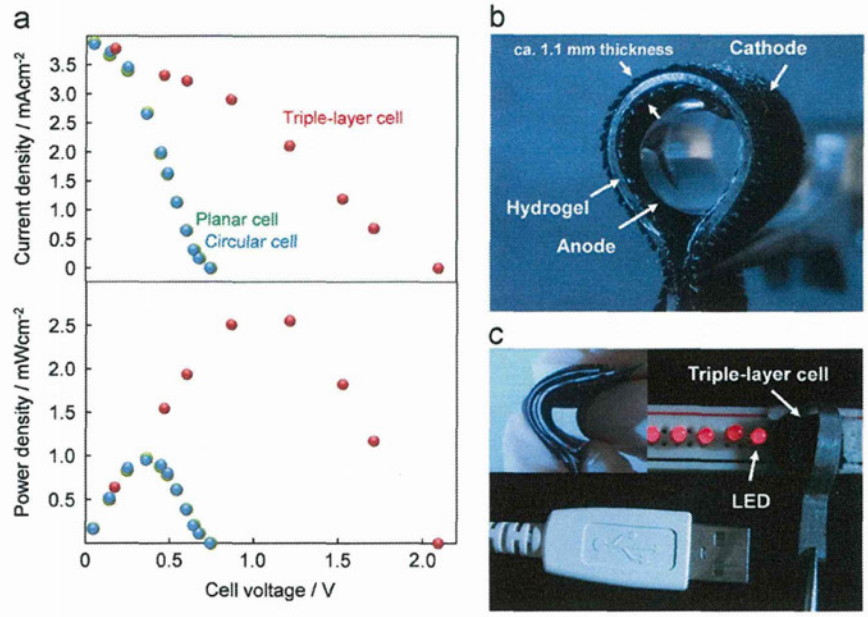

Fig. 4. (a) Performance of the biofuel cell (1 cm × 0.2 cm × 1.1 mm) with and without bending. The internal hydrogel layer was made with 250 mM McIlvaine buffer solution (pH 5.0) containing 500 mM fructose. The performance of a triple-layer cell is also shown. (b) Photograph of the biofuel cell sheet bend into a circle. (c) Photograph of the emission from LEDs connected with the triple-layer cell (inset). (For interpretation of the references to color in this figure legend, the reader is referred to the web version of this article.)

comparatively inferior activity compared to the FDH-anode fabric. The internal resistance of the cells was negligibly small, being 10 Ω hydrogel resistance and 26 Ω cell resistance measured by AC impedance spectroscopy (± 5 mV, 1–10,0000 Hz). The stability of the cells decreased extremely for few hours. Since the bioelectrodes maintained 85% performance in 500 mM fructose buffer solution (pH 5.0) for 24 h (Supporting Fig. 4), the shorter stability is due to drying of the hydrogel.

Importantly, the performance of the cell bent into an circle (blue plots) is almost identical to that of a cell that was not bent (green plots). Such high flexibility originates in the superior mechanical strength of both the fabric bioelectrodes and the DN hydrogel. As shown in Fig. 4b, the present laminar cell is thin, being only 1.12 mm thick, which also leads to a flexible character. Moreover, owing to the characteristic properties of the hydrogel, the laminar cell requires no sealing frame. Such important cell characteristics confer attractive advantage from a practical viewpoint. The application of such a laminar cell for boosting the output voltage is demonstrated in Fig. 4. The booster cell was fabricated simply by lamination of anode/hydrogel/cathode sheets (see Fig. 1d). As shown in Fig. 4a (red plots), the open-circuit voltage of the laminated cell was 2.09 V, which is 2.8-fold that of a single cell. The maximum current was quite similar to that of the single cell. These results indicate that layered cells can be connected in series without suffering from short-circuit, even without packaging. Ionic isolation between the cells could be avoided by the hydrophobicity of gas-diffusion cathodes and the solid-like property of hydrogels. The laminated cell produced a maximum power of 0.64 mW at 1.21 V (2.55 mW cm^{-2}, 6.28 mW cm^{-3}); using this level of power, we were able to light the LEDs, as demonstrated in Fig. 4c.

4. Conclusions

We have developed layered biofuel cells constructed by laminating FDH/CNT-modified CF strips, fuel-containing DN hydrogel films, and CNT/BOD/CNT-modified gas-diffusion CF strips. A single-layer cell of anode/hydrogel/cathode sheets was very thin (1.1 mm thickness), and exhibited high flexibility, being resistant to a circular bending stress. A triple-layer cell produced a higher open circuit voltage of 2.09 V corresponding to a 2.8-fold improvement over the single cell voltage (0.74 V) and a maximum power of 0.64 mW (2.55 mW cm^{-2}) at 1.21 V, indicating a successful series-connection even without packaging of each cell. It is important to note that the output voltage can easily be tuned by changing the number of layers. Such a flexible, tunable, totally organic power source could be combined in the future with wearable electronics.

Acknowlegement

The carbon fabric and carbon nanotubes were kindly donated from Toho Tenax Co. and Bayer Co., respectively. This work was partly supported by the Noguchi Institute.

Appendix A. Supporting information

Supplementary data associated with this article can be found in the online version at http://dx.doi.org/10.1016/j.bios.2012.05.041.

References

Barton, S.C., Gallaway, J., Atanassov, P., 2004. Chemical Reviews 104 (10), 86–4867.
Cooney, M.J., Svoboda, V., Lau, C., Martin, G., Minteer, S.D., 2008. Energy and Environmental Science 1 (3), 320–337.
Ferrigno, R., Stroock, A.D., Clark, T.D., Mayer, M., Whitesides, G.M., 2002. Journal of the American Chemical Society 124 (44), 12930–12931.
Gao, F., Viry, L., Maugey, M., Poulin, P., Mano, N., 2010. Nature Communications 1, 2.
Gellett, W., Kesmez, M., Schumacher, J., Akers, N., Minteer, S.D., 2010. Electroanalysis 7, 727–731.
Gong, J.P., 2010. Soft Matter. 6 (12), 2583–2590.

Haneda, K., Yoshino, S., Ofuji, T., Miyake, T., Nishizawa, M. Electrochimica Acta 1–4, in press. http://dx.doi.org/10.1016/j.electacta.2012.01.112.
Heller, A., 2004. Physical Chemistry Chemical Physics 6 (2), 209–216.
Holzinger, M., Le Goff, A., Cosnier, S. Electrochimica Acta, in press. http://dx.doi.org/10.1016/j.electacta.2011.12.135.
Miyake, T., Yoshino, S., Yamada, T., Hata, K., Nishizawa, M., 2011a. Journal of the American Chemical Society 133 (13), 5129–5134.
Miyake, T., Haneda, K., Nagai, N., Yatagawa, Y., Onami, H., Yoshino, S., Abe, T., Nishizawa, M., 2011b. Energy & Environmental Science 4, 5008–5012.
Murata, K., Kajiya, K., Nakamura, N., Ohno, H., 2009. Energy & Environmental Science 2 (12), 1280–1285.
Sakai, H., Nakagawa, T., Tokita, Y., Hatazawa, T., Ikeda, T., Tsujimura, S., Kano, K., 2009. Energy & Environmental Science 2 (1), 133–138.
Tominaga, M., Shirakihara, C., Taniguchi, I., 2007. Journal of Electroanalytical Chemistry 610 (1), 1–8.
Tominaga, M., Nomura, S., Taniguchi, I., 2009. Biosensors & bioelectronics 24 (5), 1184–1188.
Tsujimura, S., Kamitaka, Y., Kano, K., 2007. Fuel Cells 7 (6), 463–469.
Tsujimura, S., Nishina, A., Hamano, Y., Kano, K., Shiraishi, S., 2010. Electrochemistry Communications 12 (3), 446–449.
Wen, D., Xu, X., Dong, S., 2011. Energy & Environmental Science 4 (4), 1358–1363.
Willner, I., Yan, Y.-M., Willner, B., Tel-Vered, R., 2009. Fuel Cells 9 (1), 7–24.
Wu, Z.L., Gong, J.P., 2011. NPG Asia Materials 3 (6), 57–64.
Zebda, A., Gondran, C., Le Goff, A., Holzinger, M., Cinquin, P., Cosnier, S., 2011. Nature Communications 2, 370.

ADVANCED ENERGY MATERIALS
www.advenergymat.de

www.MaterialsViews.com

Molecularly Ordered Bioelectrocatalytic Composite Inside a Film of Aligned Carbon Nanotubes

*Syuhei Yoshino, Takeo Miyake, Takeo Yamada, Kenji Hata, and Matsuhiko Nishizawa**

Molecularly ordered composites of polyvinylimidazole-[Os(bipyridine)$_2$Cl] (PVI-[Os(bpy)$_2$Cl]) and glucose oxidase (GOD) are assembled inside a film of aligned carbon nanotubes. The structure of the prepared GOD/PVI-[Os(bpy)$_2$Cl]/CNT composite film is entirely uniform and stable; more than 90% bioelectrocatalytic activity could be maintained even after storage for 6 d. Owing to the ideal positional relationship achieved between enzyme, mediator, and electrode, the prepared film shows a high bioelectrocatalytic activity for glucose oxidation (ca. 15 mA cm^{-2} at 25 °C) with an extremely high electron-transfer turnover rate (ca. 650 s^{-1}) comparable to the value for GOD solutions, indicating almost every enzyme molecule entrapped within the ensemble (ca. 3×10^{12} enzymes in a 1 mm × 1 mm film) can work to the fullest extent. This free-standing, flexible composite film can be used by winding on a needle device; as an example, a self-powered sugar monitor is demonstrated.

1. Introduction

Controlling the electrical contact of redox enzymes with electrodes is a critical issue for enzymatic biodevices such as biofuel cells and biosensors.[1–12] The mutual positioning between enzyme molecules, mediator molecules (not always necessary), and electrode surface determines the efficiency, reproducibility, and stability of the bioelectrocatalysis systems. A conventional engineering for accelerating the electron transfer to the redox enzymes is inclusive immobilization with mediator polymer matrices, in which the successive electron exchange between the neighboring mediator groups connects the enzyme redox center and the electrode surface.[10–12] For example, Os-complex-pendant polymers are successful mediating matrices for glucose oxidase (GOD) and can provide glucose oxidation current at a mA cm^{-2} level.[13–16] Barton et al. reported ca. 20 mA cm^{-2} using GOD, an Os-complex polymer, and a carbon nanotube (CNT)-modified electrode.[16] However, because of random mutual positioning in the 3D composite, many enzyme molecules are isolated from the molecular network for continuous bioelectrocatalysis. On the other hand, direct immobilization of an enzyme monolayer on the electrode surface has improved the efficiency of enzyme utilization. A striking example is the reconstituting apo-GOD on a relay-FAD monolayer linked to electrode surfaces.[2,17–20] Since all the enzyme units are oriented in an optimal position with respect to the electrode surface, a high electron-transfer turnover rate comparable to that for bulk GOD reaction (approximately 700 s^{-1} at 25 °C) has been achieved. However, the drawback of such 2D monolayer engineering is the lower bioelectrocatalytic performance due to the limited amount of immobilized enzymes.

We present herein an enzyme/mediator/electrode ordered ensemble that shows both "high turnover rate" and "large catalytic current". In order to satisfy both of these requirements, the larger amount of enzymes than monolayer should be immobilized while keeping effective contact with electrodes. We realize such ideal conditions by taking advantage of a film of well-aligned carbon nanotube forest (CNTF)[21] consisting of single-walled CNTs arrayed with a pitch of 16 nm. The CNTF was synthesized by water-assisted chemical vapor deposition on a line-patterned Al_2O_3/Fe catalyst on silicon wafers (see the Experimental Section for details).[21] As shown in **Figure 1**a, the synthesized CNTF film (1.5 mm × 1 mm) was pulled from the substrate and pinched by inverse operating tweezers (electrical lead), to produce an exposed electrode geometric area of ca. 2 mm^2 (sum of both faces of a 1 mm × 1 mm sheet). The thickness of the CNTF films (4, 12, or 20μm) was determined by the width of the line-patterns of Al_2O_3/ Fe catalyst. Recently, we reported that the intraspace of the CNTF is useful for immobilization of fructose dehydrogenase and laccase, which are the direct electron transfer (DET)-type enzymes.[22] Although there are a few recent reports that also GOD is capable of direct communication with electrodes,[23–25] our repeated attempts to prepare a workable GOD/CNTF ensemble electrode without any mediators have failed. Therefore we developed a stepwise process to construct the molecular architecture with polyvinylimidazole-[Os(bipyridine)$_2$Cl] (PVI-[Os(bpy)$_2$Cl]; MW: 15 000) and GOD (EC:1.1.3.4; MW: 186 kDa), as illustrated in Figure 1b and 1c. The PVI-[Os(bpy)$_2$Cl] was synthesized according to a

S. Yoshino, Dr. T. Miyake, Prof. M. Nishizawa
Department of Bioengineering and Robotics
Tohoku University
6-6-1 Aoba, Sendai 980-8579, Japan
E-mail: nishizawa@biomems.mech.tohoku.ac.jp
Dr. T. Yamada, Dr. K. Hata
National Institute of Advanced Industrial Science and Technology (AIST)
Tsukuba Central 5, 1-1-1 Higashi, Tsukuba, Ibaraki 308-8565, Japan
Dr. T. Miyake, Dr. T. Yamada, Dr. K. Hata, Prof. M. Nishizawa
Core Research for Evolutional Science and Technology (CREST)
Japan Science and Technology Agency (JST)
Tokyo 102-0075, Japan

DOI: 10.1002/aenm.201200422

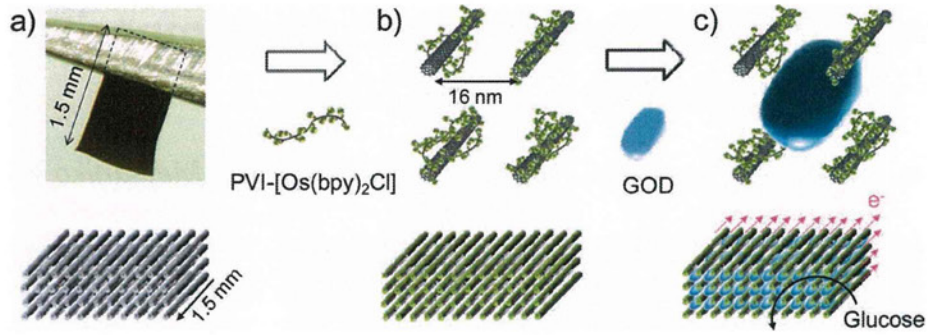

Figure 1. Schematic illustration of the stepwise process for constructing bioelectrocatalytic composite inside a CNTF film.

literature method,[26] with a molar ratio of imidazole group to $[Os(bpy)_2Cl]$ of 5.

2. Results and Discusssion

2.1. Adsorption of PVI-$[Os(bpy)_2Cl]$ inside CNTF Films

The CNTF film was first treated with 0.1% Triton X-100 to make it hydrophilic, and then soaked in a stirred phosphate buffer solution (PBS, pH 7.0) containing 1 mg mL^{-1} PVI-$[Os(bpy)_2Cl]$ at 4 °C. As shown in **Figure 2**a, the cyclic voltammogram (CV) of the treated CNTF showed a symmetric shape typical for adsorbed redox species.[27] In fact, the amplitude of peak currents were proportional to the scan rates (Figure 2b). The amount of PVI-$[Os(bpy)_2Cl]$ adsorbed within the CNTF films were estimated by integrating the CV currents and is plotted in Figure 2c against the soaking time in the 1 mg mL^{-1} PVI-$[Os(bpy)_2Cl]$ solution. The amount of PVI-$[Os(bpy)_2Cl]$ in a CNTF film increased with the soaking time and reached a maximum after 2 h. Importantly, these values are proportional to the CNTF film thickness (7.2×10^{-10} mol for a 12 μm thick film and 12.8×10^{-10} mol for a 20 μm thick film), indicating that the PVI-$[Os(bpy)_2Cl]$ molecules can entirely and uniformly adsorbed inside the CNTF films, as illustrated in Figure 1b. A part of the free imidazole groups of the mediator polymer would adsorb on CNT surfaces via π–π interaction.[28] The adsorption density of PVI-$[Os(bpy)_2Cl]$ calculated using the effective inner surface area of the CNTF films (8.2 cm^2 for 20 μm thick film)[21] was $(1.6 \pm 0.1) \times 10^{-10}$ mol cm^{-2}, which is comparable with the value for a PVI-$[Os(bpy)_2Cl]$ film adsorbed on a flat Au surface (3.2×10^{-10} mol cm^{-2}).[29]

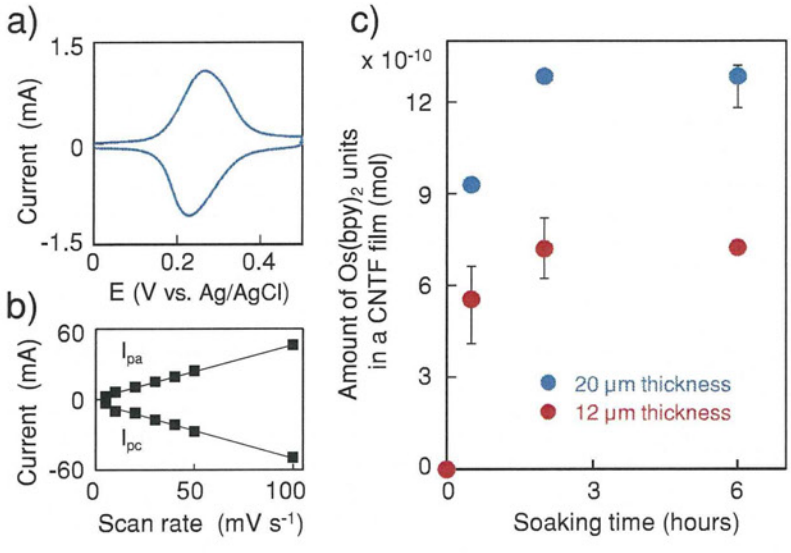

Figure 2. a) Cyclic voltammograms at 10 mV s^{-1} of the PVI-$[Os(bpy)_2Cl]$-modified CNTF film (20 μm thickness) in PBS (pH 7.0). A CNTF film was soaked in the 1 mg mL^{-1} PVI-$[Os(bpy)_2Cl]$ PBS for 6 h. b) Redox peak currents of the CVs as a function of scan rate. c) The amount of $Os(bpy)_2$ unit inside a CNTF film (film thickness: 12 and 20 μm) as a function of soaking time for 1 mg mL^{-1} PVI-$[Os(bpy)_2Cl]$ PBS solution. The mean values (± standard deviation) of three independent specimens are given.

2.2. Electrocatalytic Activity of GOD/PVI-$[Os(bpy)_2Cl]$/CNTF Ensemble Films

Subsequent loading of the enzyme GOD was conducted by immersing the PVI-$[Os(bpy)_2Cl]$-adsorbed CNTF films in a stirred PBS solution (pH 7.0) containing 3 mg ml^{-1} GOD for 1 hour. **Figure 3**a shows the CVs of GOD/PVI-$[Os(bpy)_2Cl]$/CNTF ensemble films at 10 mV s^{-1} in a stirred 200 mM D-glucose PBS solution. The catalytic current for glucose oxidation increased in response to the thickness of CNTF films (3.7 mA cm^{-2} for 4 μm thickness and 14.7 mA cm^{-2} for 20 μm thickness), indicating that also GOD can entirely penetrate inside the PVI-$[Os(bpy)_2Cl]$-modified CNTF films. For example, the content of GOD incorporated in a 20 μm thick film was measured as ca. 0.86 μg by a C-6667 Protein Quantitation Kit, the value being a little below the case when GOD molecules ($6.7 \times 6.7 \times 21$ nm^3)[30] align to form lines in the interspace of CNTs (1.17 μg). The current density under stirred condition was enhanced to as high as 26.7 mA cm^{-2} by turning up the buffer temperature to 37.5 °C. This glucose

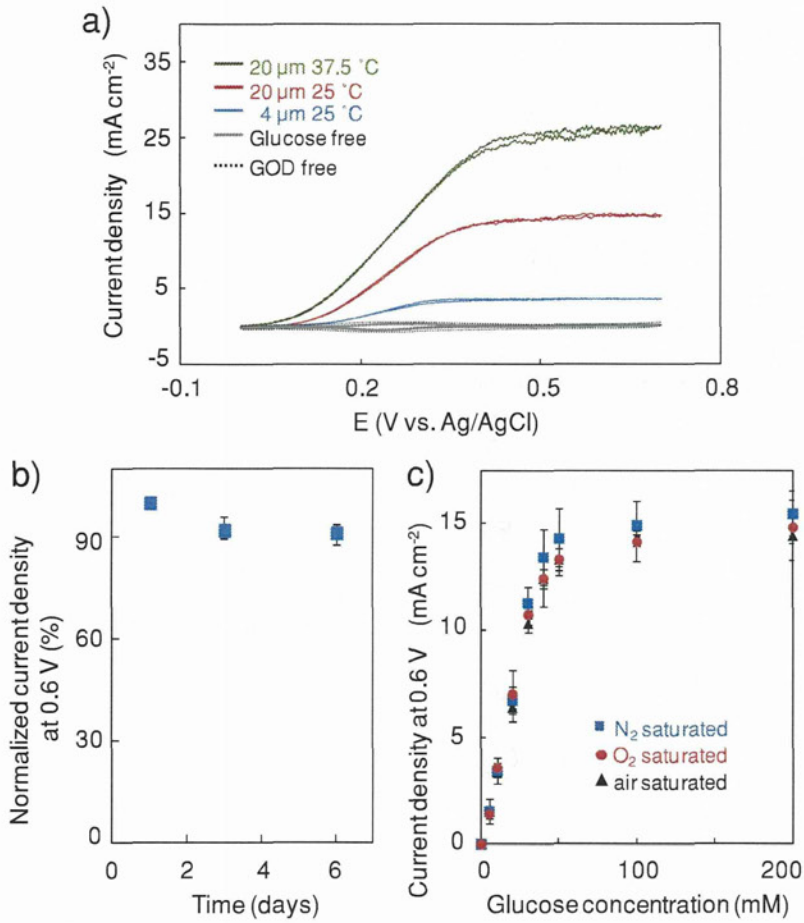

Figure 3. a) Cyclic voltammograms of GOD/PVI-Os/CNTF ensemble films at 10 mV s^{-1} in stirred air-saturated 25 °C (or 37.5 °C) PBS containing 200 mM-glucose. The thicknesses of CNTF films were 4 or 20 µm. The control voltammograms without GOD and glucose are also shown. We used a total geometric area of the pinched film (2 mm^2) for the calculation of the current densities. b) The oxidation current densities at 0.6 V vs. Ag/AgCl for the GOD/PVI-[Os(bby)$_2$Cl]/CNTF film (20 µm thickness) in a stirred 200 mM-glucose PBS solution, periodically measured during 6 d of storage in PBS solution. c) The current densities at 0.6 V for the 20 µm GOD/PVI-[Os(bby)$_2$Cl]/CNTF film as a function of the glucose concentration, measured in O_2-, N_2-, and air-saturated stirred PBS (pH 7.0) solutions. The mean values (± standard deviation) of three independent specimens are given.

oxidation activity is comparable or superior to those previously reported using GOD.[13–16] In a quiescent condition, the current density decreased by half, probably due to the limited mass-transfer inside the film. Importantly, more than 90% of the electrode activity could be maintained even after 6 d storage in an air-saturated PBS solution (Figure 3b), proving the stability of bioelectrocatalytic architecture with the composite of PVI-[Os(bpy)$_2$Cl] polymer and GOD. The anionic GOD molecules could be stably entrapped by electrostatic interaction with cationic Os-complex of the mediator polymer that is anchored on the CNT surface via π–π interaction.[28]

The electron-transfer turnover rate for the 20 µm thick film was calculated from the current value at 25 °C (0.29 mA), the Faraday constant (96 500 C mol^{-1}), the molecular weight of GOD (186 000 g mol^{-1}), and the content of GOD molecules in a piece of the ensemble film (ca. 0.86 µg). The derived averaged turnover rate was ca. 650 s^{-1}, being comparable to that of GOD in bulk solution containing the natural electron acceptor O_2 (700 s^{-1}) at 25 °C.[31] These results indicate that most of ca. 3×10^{12} GOD units within the film could efficiently work to the fullest extent, presumably owing to the molecularly ordered structure of enzyme/mediator/electrode ensemble. Such a high efficiency of the present GOD electrode resulted in a resistance to oxygen inhibition, as shown in Figure 3c. The catalytic performance was almost identical in N_2-saturated, air-saturated, and even O_2-saturated solutions. In general, glucose oxidation with GOD-modified electrodes is often disturbed by dissolved O_2, which is troublesome for glucose sensing.[32,33] However, the ordered Os(bby)$_2$ groups in the present ensemble electrode could effectively accept the electron from GOD in preference to O_2, resulted in excellent O_2 resistance.

2.3. Application as a Flexible Anode of Biofuel Cells

The present free-standing, bioelectrocatalytic film could be used for miniature biofuel cell devices. We demonstrate here the application of the film to a self-powered sugar indicator designed for inserting into a fruit. For indicating the glucose concentration, the net performance of the biofuel cell system should be controlled by the glucose anode. Because the oxygen in fruits is limited to a lower concentration than glucose, we employ a gas-diffusion biocathode[34] for utilizing the abundant oxygen in air outside of the fruits (see the Experimental Section for details). **Figure 4**a shows the biofuel cell performance measured using 200 mM glucose PBS solution with a couple consisting of a GOD/PVI-[Os(bby)$_2$Cl]/CNTF film anode (20 µm thickness) and a cathode made from bilirubin oxidase (BOD)-modified carbon fabric (1 cm × 1 cm). The open-circuit voltage of the cell was 0.5 V in agreement with the difference between the potentials at which glucose oxidation and oxygen reduction start to occur in cyclic voltammetry (0.1 V in Figure 3a and 0.6 V in Figure S1, see the Supporting Information). The maximum output current (0.27 mA) is almost equivalent to the maximum oxidation current at the composite anode (0.29 mA) that can be calculated by the current density in Figure 3a (14.7 mA cm^{-2}) and the electrode area of 2 mm^2. This result indicates that the system is limited by the anode even in 200 mM glucose, a concentration that is markedly higher than that found in raw fruits (a few tens of mM). As shown in Figure 4b, a piece of GOD/PVI-[Os(bby)$_2$Cl]/CNTF film was wound on one lead of a light-emitting-diode (LED) device, whose blinking interval is inversely proportional

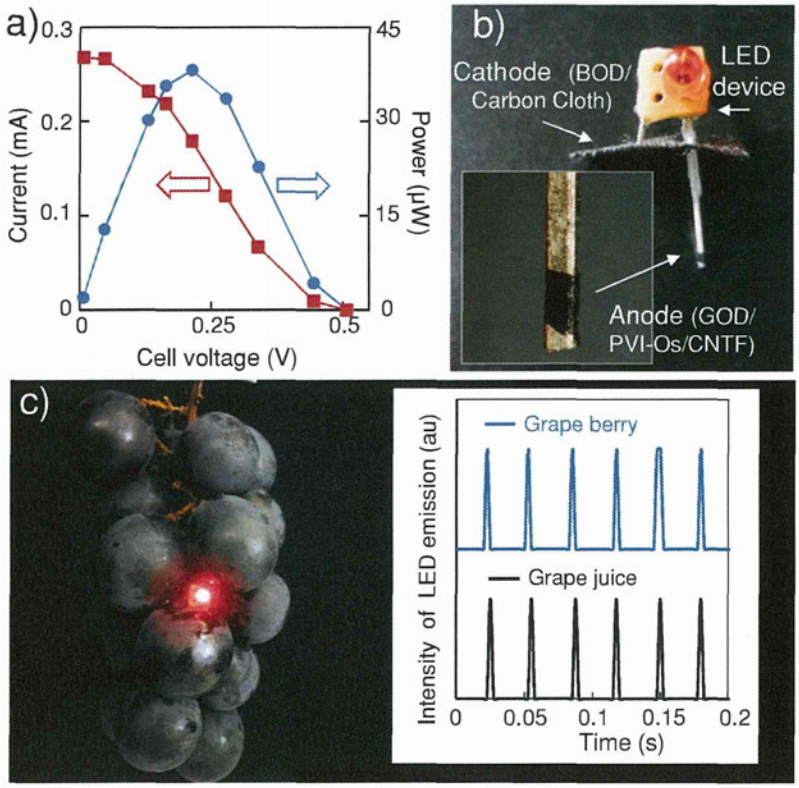

Figure 4. a) Performance of a biofuel cell composed of an anode of GOD/PVI-[Os(bby)$_2$Cl]/CNTF film (20 μm thickness) and a cathode of BOD-modified carbon cloth (1 cm × 1 cm) in 200 mM glucose PBS solution, measured by changing the external resistance (28 to 46kΩ). b) Photograph of the LED-based self-powered sugar indicator, at the tip of which the GOD/PVI-[Os(bby)$_2$Cl]/CNTF film was wound. c) The device assembly was inserted in a grape and the LED blinking was measured (inset). The time course of LED emission, taken using an extracted juice, is also shown.

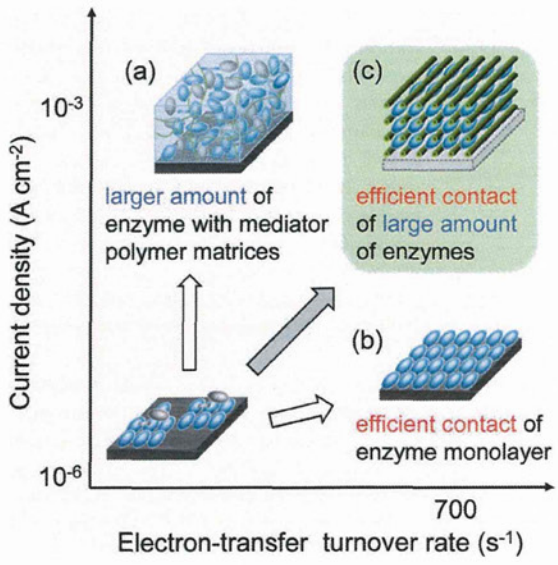

Figure 5. Scheme showing correlative characters of: a) an enzyme-film with mediator polymer matrices for larger current, b) an enzyme-monolayer electrode for higher turnover rate, and, c) the present ensemble electrode for both large current and high turnover rate.

to the power of the biofuel cell.[35,36] The other lead was connected to the BOD-based gas-diffusion cathode. The blinking interval of the LED upon inserting the device to a grape was coincident with that for the extracted juice (Figure 4c), proving that this device could serve as a sugar indicator by simply being inserted into a grape. We confirmed that there is no corrosion reaction at the LED lead wire during the operation. The present principle of the self-powered sensor could be applied to more important blood sugar monitoring applications; we are planning to develop a GOD/PVI-[Os(bby)$_2$Cl]/CNTF-based device structure suitable for low-invasive insertion into a blood vessel through skins.

3. Conclusions

An amount of enzyme units larger than that in a monolayer were successfully immobilized while keeping effective electrical contact with the electrode (CNTs), as summarized in **Figure 5**. In particular, we have succeeded in forming an entirely uniform bioelectrocatalytic architecture with PVI-[Os(bby)$_2$Cl] and GOD inside a CNTF film. The voltammograms of the PVI-[Os(bby)$_2$Cl]-modified CNTF indicated the uniform adsorption of PVI-[Os(bpy)$_2$Cl] on the CNT surface via π–π interaction with the density of ca. $(1.6 \pm 0.1) \times 10^{-10}$ mol cm^{-2}. The subsequent GOD seemed to become stably entrapped at the interspaces of PVI-[Os(bby)$_2$Cl]-modified CNTs by the electrostatic interaction. Owing to the ordered positional relationship between GOD, PVI-[Os(bby)$_2$Cl], and CNT, the composite film showed both high activity for glucose oxidation (ca. 15 mA cm^{-2}) and high electron-transfer turnover rate (ca. 650 s^{-1}), indicating almost every enzyme molecules within the film could work to the fullest extent.

4. Experimental Section

CNTF Preparation: CNTF was synthesized in a 1 inch tube furnace by water-assisted chemical vapor deposition at 750 °C with a C_2H_4 carbon source and an Al_2O_3 (10 nm)/Fe (1.0 nm) thin-film catalyst grown on silicon wafers.[21] We used He with H_2 as the carrier gas (total flow 1000 standard cubic centimeters per minute (sccm)) at 1 atm with a controlled amount of water vapor with ethylene (100 sccm) for 10 min.

Quantitative Analysis of the Entrapped Enzymes: The quantitative analysis of GOD was conducted as explained in our previous paper.[22] The enzyme-incorporated CNTF film was first washed and immersed in 20 mM sodium phosphate buffer (pH 9.3) containing 0.1 M sodium borate and 1% sodium cholate and dispersed with an ultrasonic homogenizer for 15 min. The GOD in the dispersion was then analyzed using a C-6667 Protein Quantitation Kit (Molecular Probes), using 5 mM (3-(4-carboxybenzoyl)-quinoline-2-carboxaldehyde) (ATTO-TAG CBQCA) and 20 mM KCN to label the enzyme with CBQCA. After 1.5 h of incubation, the fluorescent intensity was measured by a luminescent

image analyzer system (Fuji Photo Film, LAS-3000 mini), and the amount of enzyme was determined by referencing a calibration curve.

Preparation of Gas-diffusion Carbon Fabric (CF) Cathodes: The preparation of the cathode basically followed the procedures used for our previous work.[34] A 40 µL aliquot of a 10 mg mL^{-1} multiwalled CNT solution was put on a CF strip and dried in air, followed by thoroughly washing out the surfactant by soaking in an ethanol solution for more than 1 h with stirring. The surface of the CNT-modified CF electrode was further modified with a 0.1 mL solution of 5 mg mL^{-1} bilirubin oxidase (BOD, EC 1.3.3.5, 2.5 U mg^{-1}, from Myrothecium) in a vacuum oven (0.09 MPa, 35 °C). The strip was additionally coated with the CNT solution to make the surface hydrophobic.

Electrochemical Measurements: The GOD/PVI-[$Os(bpy)_2Cl$]/CNTF ensemble films, anchored at the edge with SUS316L fine tweezers, was analyzed by a three-electrode system (BSA, 730C electrochemical analyzer) in stirred solutions using a Ag/AgCl reference and a platinum counter electrode. The gas-diffusion cathode (BOD-modified CF strip) was put on an air-saturated solution so as to contact the solution by the BOD-modified face during cyclic voltammetry (Figure S1 in the Supporting Information). The performance of a biofuel cell constructed from an GOD-based CNTF anode and an BOD-based CF cathode was evaluated on the basis of the cell voltage upon changing the external resistance between 1 kΩ and 2 MΩ at the time step of 60 s. Unless otherwise indicated, the electrochemical measurements were carried out at room temperature (25 °C).

Supporting Information

Supporting Information is available from the Wiley Online Library or from the author.

Acknowledgements

Authors express appreciation to Toho Tenax Co. for donation of the carbon fabrics and to Bayer Co. for multiwalled carbon nanotubes.

Received: June 8, 2012
Revised: June 29, 2012
Published online: August 24, 2012

[1] I. Willner, Z. Katz, *Bioelectronics*, Wiley-VCH,Weinheim Germany **2005.**
[2] I. Willner, Y. M. Yan, B. Willner, R. Tel-Vered, *Fuel Cells* **2009**, *1*, 7.
[3] G. T. R. Palmore, H. Bertschy, S. H. Bergens, G. M. Whitesides, *J. Electroanal. Chem.* **1998**, *443*, 155.
[4] R. L. Arechederra, S. D. Minteer, *Fuel Cells* **2009**, *1*, 63.
[5] W. Gellett, M Kesmez, J. Schumacher, N. Akers, S. D. Minteer, *Electroanalysis* **2010**, *22*, 727.
[6] S. D. Minteer, P. Atanassov, H. R. Luckarift, G. R. Johnson, *Mater. Today* **2012**, *15*, 166.
[7] L. Halámková, J. Halámek, V. Bocharova, A. Szczupak, L. Alfonta, E. Katz, *J. Am. Chem. Soc.* **2012**, *134*, 5040.
[8] D. Leecha, P. Kavanagha, W. Schuhmann, *Electrochim. Acta* **2012**, DOI:10.1016/j.electacta.2012.02.087.
[9] M. Holzinger, A. L. Goff, S. Cosnier, *Electrochim. Acta* **2012**, DOI:10.1016/j.electacta.2011.12.135.
[10] A. Heller, B. Feldman, *Acc. Chem. Res.* **2010**, *43*, 963.
[11] S. G. Barton, J. Gallaway, P. Atanassov, *Chem. Rev.* **2004**, *104*, 4867.
[12] W. Schuhmann, T. J. Ohara, H. L. Schmidt, A. Heller, *J. Am. Chem. Soc.* **1991**, *113*, 1394.
[13] F. Mao, N. Mano, A. Heller, *J. Am. Chem. Soc.* **2003**, *125*, 4951.
[14] F. Gao, L. Viry, M. Maugey, P. Poulin, N. Mano, *Nat. Commun.* **2010**, *1*, 2.
[15] H. Wen, V. Nallathambi, D. Chakraborty, S. C. Barton, *Microchim. Acta* **2011**, *175*, 283.
[16] S. C. Barton, Y. Sun, B. Chandra, S. White, J. Hone, *Electrochem. Solid-State Lett.* **2007**, *10*, B96.
[17] Y. Xiao, F. Patolsky, E. Katz, J. F. Hainfeld, I. Willner, *Science* **2003**, *299*, 1877.
[18] F. Patolsky, Y. Weizmann, I. Willner, *Angew. Chem., Int. Ed.* **2004**, *43*, 2113.
[19] M. Zayats, E. Katz, I. Willner, *J. Am. Chem. Soc.* **2002**, *124*, 2120.
[20] I. Willner, V. Heleg-Shabtai, R. Blonder, E. Katz, G. Tao, A.F. Bückmann, A. Heller, *J. Am. Chem. Soc.* **1996**, *118*, 10321.
[21] D. N. Futaba, K. Hata, T. Yamada, T. Hiraoka, Y. Hayamizu, Y. Kakudate, O. Tanaike, H. Hatori, M. Yumura, S. Iijima, *Nat. Mater.* **2006**, *5*, 987.
[22] T. Miyake, S. Yoshino, T. Yamada, K. Hata, M. Nishizawa, *J. Am. Chem. Soc.* **2011**, *133*, 5129.
[23] A. Guiseppi-Elie, C. Lei, R. H. Baughman, *Nanotechnology* **2002**, *13*, 559.
[24] A. Zebda, C. Gondran, A. L. Goff, M. Holzinger, P. Cinquin, S. Cosnier, *Nat. Commun.* **2011**, *2*, 1.
[25] J. T. Holland, C. Lau, S. Brozik, P. Atanassov, S. J. Banta, J. *Am. Chem. Soc.* **2011**, *133*, 19262.
[26] T. J. Ohara, R. Rajagopalan, A. Heller, *Anal. Chem.* **1993**, *65*, 3512.
[27] A. J. Bard, L. R. Faulkner, *Electrochemical Methods: Fundamental and Applications*, Wiley, New York, 2001, 589.
[28] T. Roman, W. A. Dino, H. Nakanish, H. Kasai, *Eur. Phys. J. D* **2006**, *38*, 117.
[29] Y. Wang, P. P. Joshi, K. L. Hobbs, M. B. Johnson, D. W. Schmidtke, *Langmuir* **2006**, *22*, 9776.
[30] G. Wohlfahrt, S. Witt, J. Hendle, D. Schomburg, H. M. Kalisz, H. Hecht, *J. Acta Cryst., Sect. D: Biol. Crystallogr.* **1999**, *D55*, 969.
[31] C. Bourdillon, C. Demaille, J. Gueris, J. Moiroux, J. M. Savebant, *J. Am. Chem. Soc.* **1993**, *115*, 12264.
[32] J. Wang, *Electroanalysis* **2001**, *13*, 983.
[33] B. A. Gregg, A. Heller, *Anal. Chem.* **1990**, *62*, 258.
[34] K. Haneda, S. Yoshino, T. Ofuji1, T. Miyake, M. Nishizawa, *Electrochim. Acta* **2012**, DOI: 10.1016/j.electacta.2012.01.112.
[35] T. Hanashi, T. Yamazaki, W. Tsugawa, S. Ferri, D. Nakayama, M. Tomiyama, K. Ikebukuro, K. Sode, *Biosens. Bioelectron.* **2009**, *24*, 1837.
[36] T. Miyake, K. Haneda, N. Nagai, Y. Yatagawa, H. Onami, S. Yoshino, T. Abe, M. Nishizawa, *Energy Environ. Sci.* **2011**, *4*, 5008.

Spatiotemporally controlled contraction of micropatterned skeletal muscle cells on a hydrogel sheet†

Kuniaki Nagamine,[ab] Takeaki Kawashima,[a] Soichiro Sekine,[a] Yuichiro Ido,[a] Makoto Kanzaki[bc] and Matsuhiko Nishizawa*[ab]

Received 1st September 2010, Accepted 3rd November 2010
DOI: 10.1039/c0lc00364f

We have developed gel sheet-supported C_2C_{12} myotube micropatterns and combined them with a microelectrode array chip to afford a skeletal muscle cell-based bioassay system. Myotube line patterns cultured on a glass substrate were transferred with 100% efficiency to the surface of fibrin gel sheets. The contractile behavior of each myotube line pattern on the gel was individually controlled by localized electrical stimulation using microelectrode arrays that had been previously modified with electropolymerized poly(3,4-ethylenedioxythiophene) (PEDOT). We successfully demonstrated fluorescent imaging of the contraction-induced translocation of the glucose transporter, GLUT4, from intracellular vesicles to the plasma membrane of the myotubes. This device is applicable for the bioassay of contraction-induced metabolic alterations in a skeletal muscle cell.

Introduction

In vitro bioassay systems incorporating cells with physiological activity have been developed as an alternative to whole animal experiments.[1,2] Systems using skeletal muscle cells are one of the promising devices to reveal the complex mechanisms of type 2 diabetes because that disease is associated with a disorder of insulin- or contraction-induced glucose metabolism in a skeletal muscle cell *in vivo*.[3,4] Such a bioassay system could be also useful for screening candidate drugs against type 2 diabetes.

Bioassay systems fabricated by combining microelectric devices with cell-micropatterning techniques have enabled localized electrical regulation and long-term monitoring of electrophysiological responses from cells such as neural, cardiac, and skeletal muscle cells cultured on the device.[5–12] However, it is difficult to culture fully differentiated cells and to maintain their physiological activity on the solid devices. Specifically, there are few reports on devices combined with electrically excitable contractile skeletal muscle cell culture because the cells readily detached from the substrate within a few days.[13] For a stable bioassay device, it is necessary to develop an on-device culture method of fully differentiated cells, while sustaining their activity for long periods.

Recently, to overcome the difficulties associated with on-device cultivation, a manipulatable cell sheet which is composed of confluent cell monolayers and a flexible polymer sheet has been developed.[14–17] The cell sheet can be handled while sustaining the cellular structure and activity and it can be combined with the devices on demand. We have developed gel sheet-supported contractile C_2C_{12} myotube micropatterns by means of the cell transfer technique (Fig. 1(A)).[17] Micropatterned myotubes/gel sheet was prepared by transferring the myotube line patterns cultured on a glass substrate onto the surface of fibrin gel sheet with 100% efficiency. Myotubes on the gel sheet exhibited longer-term contractile activity without detachment from the gel than the cells on a conventional solid culture dish.

In the present study, we patched the myotube/fibrin gel sheet onto a microelectrode array chip to construct a skeletal muscle cell-based bioassay device (Fig. 1(B)). The Pt microelectrode arrays were previously coated with a conducting polymer, poly(3,4-ethylenedioxythiophene) (PEDOT), that has a large electroactive surface area due to its fibrous structure. This modification increases the interfacial electrical capacity of the electrodes and ensures a less invasive electrical stimulation of the cells without causing faradaic reactions and gas evolution.[18]

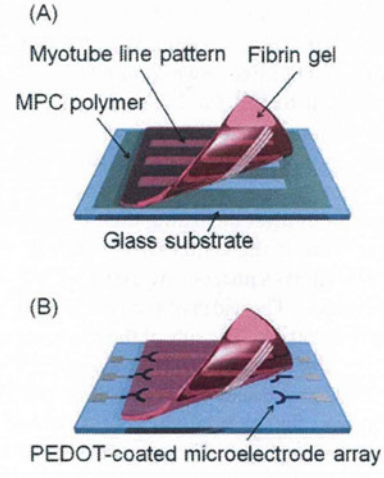

Fig. 1 Overview of the myotube/fibrin gel sheet combined with the PEDOT microelectrode array chip. (A) Cell transfer from a glass substrate to a fibrin gel. (B) Attachment of the myotube/fibrin gel onto the microelectrode arrays.

[a]*Department of Bioengineering and Robotics, Graduate School of Engineering, Tohoku University, 6-6-01 Aramaki, Aoba-ku, Sendai, 980-8579, Japan. E-mail: nishizawa@biomems.mech.tohoku.ac.jp; Fax: +81 22 795 7003; Tel: +81 22 795 7003*
[b]*JST-CREST, Sanbancho, Chiyoda-ku, Tokyo, 102-0075, Japan*
[c]*Department of Biomedical Engineering, Graduate School of Biomedical Engineering, Tohoku University, Biomedical BLD, 2-1 Seiryo-machi, Aoba-ku, Sendai, 980-8575, Japan*

† Electronic supplementary information (ESI) available: Movie 1 and 2. See DOI: 10.1039/c0lc00364f

The usefulness of this device for type 2 diabetes researches was demonstrated by fluorescent imaging of the contraction-induced translocation of the glucose transporter, GLUT4, from intracellular vesicles to the plasma membrane of the myotubes. GLUT4 is a principal mediator of glucose uptake in the skeletal muscle cell in response to insulin and contraction. GLUT4 distributes in the intracellular region under unstimulated state, and is transported to the plasma membrane in response to these stimuli to accelerate glucose uptake in the cells. Defection in stimuli-responsive GLUT4 translocation is closely associated with the development of type 2 diabetes, which is supported by the whole animal experiments.[3,4]

Experimental

Contractile C_2C_{12} myotube micropatterns on a fibrin gel

Wild type (WT)-C_2C_{12} myoblasts (less than six passages in age; American Type Culture Collection, Manassas, VA, USA) were cultured on a glass substrate with a line-patterned cell-resistant polymer, 2-methacryloyloxyethyl phosphorylcholine (MPC, Lipidure-CM5206E, NOF Corp., Tokyo, Japan) at 37 °C, under a 5% CO_2 atmosphere in a growth medium composed of Dulbecco's modified Eagle's medium (DMEM, Wako Pure Chemicals Industries, Ltd, Osaka, Japan) containing 10% fetal bovine serum (BioWest, Nuaille, France), 100 units mL^{-1} penicillin, and 100 μg mL^{-1} streptomycin (Invitrogen Corp., Carlsbad, CA, USA) until fully confluent. Myoblasts were induced to differentiate into myotubes by replacing the growth medium with a differentiation medium composed of DMEM containing 2% calf serum (Thermo Electron Corporation, Melbourne, Australia), 1 nM insulin (Sigma-Aldrich, St Louis, MO, USA), 100 units mL^{-1} penicillin, and 100 μg mL^{-1} streptomycin.

Then, the myotubes were transferred onto a fibrin gel. The fibrinogen mixture solution was prepared by dissolving 15 mg mL^{-1} fibrinogen (Sigma-Aldrich), 0.5 mg mL^{-1} aprotinin (Sigma-Aldrich), and 10 U mL^{-1} thrombin (Ito Life Science, Inc., Ibaraki, Japan) in an electrical pulse stimulation (EPS) medium composed of DMEM containing 2% calf serum, 2% MEM amino acids solution (Invitrogen Corp.), 1% MEM non-essential amino acids solution (Invitrogen Corp.), 100 units mL^{-1} penicillin, and 100 μg mL^{-1} streptomycin. The mixture was poured over the cells, and the culture was left undisturbed for 2 h at 37 °C under a 5% CO_2 atmosphere to facilitate fibrin gelation and to allow the cells to adhere on the surface of the gel. Fig. 2(A) shows a photograph of the fibrin gel sheet (size, 1 cm × 1 cm; thickness, 2 mm) with myotube line patterns after detaching the gel from the substrate. The white lines seen at the center of the gel are myotube line patterns. Fig. 2(B) shows a phase-contrast micrograph of myotube line patterns on the gel. The width of each line and the gap between the lines were set at 250 μm. The side of the fibrin gel sheet with the attached myotubes was covered with an additional thin fibrin gel layer (less than 100 μm) because we found that the additional gel layer was effective for maintaining the structure of cellular micropatterns for a long term. The myotube/fibrin gel was finally placed in a carbon electrode chamber (C-Pace 100, IonOptix, Milton, MA, USA) and periodic electrical pulses (amplitude, 0.7 V mm^{-1}; frequency, 1 Hz; duration, 2 ms) were applied for 4 days in the EPS medium to endow the cells with contractile activity.[17]

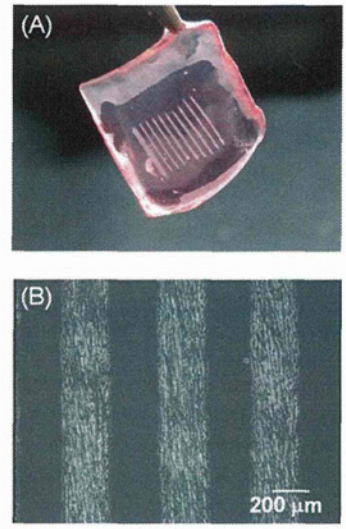

Fig. 2 (A) Photograph of a fibrin gel with myotube line patterns. (B) Phase-contrast micrograph of myotube line patterns on the gel.

Conducting polymer-coated Pt microelectrode arrays

Pt microelectrode arrays were fabricated on a glass substrate using conventional photolithography and lift-off techniques. Electropolymerization of poly(3,4-ethylenedioxythiophene) (PEDOT) on the microelectrode surfaces was carried out for 1 min in an aqueous solution containing 50 mM 3,4-ethylenedioxythiophene (Sigma-Aldrich) as a monomer and 100 mM KNO_3 as a dopant under potentiostatic conditions at +1.0 V *vs.* Ag/AgCl. Thickness of the PEDOT layer on the electrode was 467 ± 22 nm (n = 5) measured using a surface profiler (P-10, KLA-Tencor, CA, USA).

The contractile myotube/fibrin gel sheet was placed on the PEDOT microelectrode arrays so that the side of the gel sheet with the attached myotubes was in contact with the electrode surface. The myotube line patterns were carefully aligned with the microelectrode patterns using tweezers under microscopic observation. Periodic electrical pulses were applied between the desired microelectrode pairs to induce myotube contraction in the EPS medium.

GLUT4 translocation assay by immunostaining

Transfected C_2C_{12} myotube stably expressing rat GLUT4, with a c-myc epitope tag in the first extracellular loop and an enhanced cyan fluorescent protein (ECFP) at the carboxyl terminus, was used to detect membrane-bound GLUT4 using an anti-c-myc antibody.[19,20] WT- and transfected myoblasts mixed at a 1 : 1 ratio were grown and differentiated on a MPC polymer patterned substrate[19,20] and transferred onto a fibrin gel as described above. The myotubes were electrically stimulated using the carbon electrode chamber for 4 days to endow the cells with contractile activity. Then, the gel sheet was placed on the PEDOT microelectrode arrays for localized electrical stimulation of arbitral myotube line pattern for 3.5 h (amplitude, 2 V; duration, 3 ms; frequency, 10 Hz; train, 1 s; interval, 10 s) in the EPS medium. After that, the cells were fixed with 1% *p*-formaldehyde (Electron Microscopy Sciences, Fort Washington, PA,

USA) in PBS(−). The blocking step was carried out using 5% calf serum in PBS(−) to avoid non-specific adsorption of the antibody and reduce the background signal. In fact, there was no significant non-specific binding of mouse IgG antibody against myotubes assessed by the enzyme-linked immunosorbent assay. The cells were immunostained using the mouse monoclonal anti-c-myc first antibody (Santa Cruz Biotechnology, Santa Cruz, CA, USA) overnight at 4 °C. Then, Alexa Fluor 594-conjugated anti-mouse IgG second antibody (Invitrogen Corp.) was bound to the first antibody for 1 h at room temperature. The immunostained gel sheet was mounted on a cover glass with Vectashield (Vector Laboratories, Burlingame, CA, USA). Fluorescent images were observed using a LSM 700 laser scanning microscope and the associated LSM software, ZEN 2009 (Carl Zeiss MicroImaging Co., Ltd, Tokyo, Japan).

Results and discussion

To achieve long-term minimally invasive stimulation of muscle cells, the electrodes were coated with PEDOT. Fig. 3 shows the micrographs of bare (A and B) and PEDOT-coated Pt microelectrodes (C and D). It is clear that the white shiny bare Pt microelectrode surface (A) was changed to black by the PEDOT modification (C). After the electrical pulse application (amplitude, 2 V; frequency, 1 Hz; duration, 10 ms) for 15 h in the EPS medium, the color of the bare Pt microelectrode changed to brown (B). This discoloration would be attributed to the electrochemical corrosion of the Pt layer, which means oxidation of the Pt layer at a high potential pulse cycle, followed by dissolution as the Pt ion into the medium.[21] On the other hand, the PEDOT-coated microelectrode showed no apparent morphological change even after 15 h of pulse application (Fig. 3(D)), and remained intact for more than 3 days pulse application. The PEDOT film of the electrode (D) was removed by aqueous sodium hypochlorite which causes over-oxidation and degradation of the PEDOT film,[22] which revealed that the underlying Pt microelectrodes remained intact (Fig. 3(E)). In addition to corrosion of the Pt layer, the faradaic reactions at the Pt electrode/medium interface cause drastic changes in culture conditions such as pH, which would injure the cells. In fact, we observed gas evolution, which was associated with water electrolysis at the bare Pt electrode, resulted in damaging the cells on the electrodes.[18] When using the PEDOT-coated microelectrode with a large surface electric capacity, the non-faradaic charging current will suppress unfavorable faradaic reactions and ensure stable long-term electric stimulation.

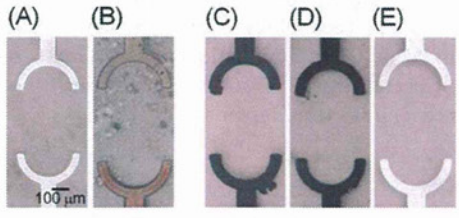

Fig. 3 Micrographs of bare (A and B) and PEDOT-coated Pt microelectrodes (C and D) before (A and C) and after (B and D) electrical pulse application (amplitude, 2 V; frequency, 1 Hz; duration, 10 ms) for 15 h in the EPS medium. (E) Pt microelectrode after detachment of PEDOT layer from the electrode D.

The electric field distribution on the microelectrode array was simulated by the finite element method using FEMLAB software (COMSOL 3.1, COMSOL AB, Sweden). The three-dimensional model geometry, including microelectrode arrays, mimicked those of the experimental setup. The simulated model microelectrode arrays did not include the electrode material properties. Fig. 4(A) shows a micrograph of the PEDOT microelectrode arrays and Fig. 4(B) shows the simulated electric field distribution for a model microelectrode array when a voltage of 2 V was applied between the central microelectrode pair. The electric field was concentrated between the active electrodes and did not spread out to the neighbouring regions. Fig. 4(C) shows the electric field distribution along the cross-section a–b in Fig. 4(B). The vertical axis in Fig. 4(C) represents the distance from the microelectrode surface. The simulated electric field rapidly decreased with increasing distance from the microelectrode surface. These data suggested that the electric field generated by the microelectrodes was effective only in the region near the microelectrode surface. Assuming the vertical axis in Fig. 4(C) to be the thickness of the gel, for effective electrical stimulation the myotubes/fibrin gel should be attached to the microelectrode array chip so that the side of the gel sheet with the transferred myotubes was in contact with the electrode surface.

Fig. 5(A) shows a phase-contrast micrograph of WT-C_2C_{12} myotube line patterns on the fibrin gel aligned with the PEDOT microelectrode arrays. During the alignment, the lined structure of the myotubes was maintained without detachment from the gel, allowing arbitrary and repetitive changes of the localized electrical stimulation site on the myotube line patterns. As can be seen in Fig. 5(A), the focus on the cells was matched with that of on the microelectrodes, suggesting the cells are in close vicinity of the electrode surface. The distance between the cells and the PEDOT layer was less than 100 μm, as assessed from the defocusing Z distance using a confocal microscopy. Fig. 5(B) shows the time courses of contractile displacements of myotube line patterns on the PEDOT microelectrode arrays when stimulated with periodic electrical pulses (amplitude, 2 V; frequency, 1 Hz; duration, 10 ms). Contractile displacement was determined from the real-time movie of myotube contraction shown in Movie S1, ESI†.

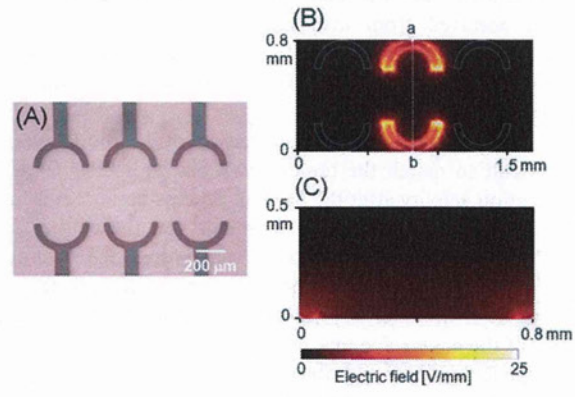

Fig. 4 (A) Micrograph of the PEDOT-coated microelectrode arrays. (B) Simulated electric field distribution for a model microelectrode array where a voltage of 2 V was applied between the central microelectrode pair. (C) Simulated electric field distribution along the cross-section a–b in (B).

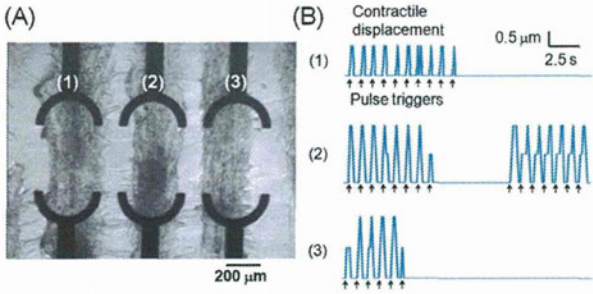

Fig. 5 (A) Phase-contrast micrograph of WT-C_2C_{12} myotube line patterns aligned with the microelectrode arrays. (B) Time course of myotube line patterns contraction stimulated with periodic electrical pulses (amplitude, 2 V; frequency, 1 Hz; duration, 10 ms). The arrows below the time course represent the pulse triggers.

Pulse triggers are indicated as arrows below each time course. The numbers (1) to (3) in Fig. 5(B) represent the contractile behavior of myotube line patterns labeled (1) to (3) in Fig. 5(A). At first, all the myotube line patterns were stimulated, followed by resting patterns (3) to (1) in order, and finally we selectively stimulated just pattern (2). Each myotube line pattern exhibited independent contractile behaviour synchronized with the electric pulse supplied through the aligned microelectrodes. These results suggested that contractile activity of each myotube line pattern could be arbitrarily controlled using the microelectrode arrays.

Fig. 6 depicts the expression assay of GLUT4 by the selective stimulation of the transfected myotube line patterns. Myotube line pattern on the left side was stimulated for 3.5 h at 10 Hz (amplitude, 2 V; duration, 3 ms; train, 1 s; interval, 10 s) and the right side pattern was rested, as shown in Movie S2, ESI†. The myotubes were immunostained with the anti-c-myc first antibody and the Alexa Fluor 594-conjugated anti-mouse IgG second antibody after the electrical stimulation and cell fixation. The antibodies used are impermeable to the cell membrane, which makes it enable to stain only the GLUT4 expressed on the cell surface.[19] As can be seen in Fig. 6(B) and (C), electrically stimulated myotubes displayed an obvious increase in fluorescent intensity above that of unstimulated cells by about 4-fold. This result suggests that the contraction-induced GLUT4 translocation occurred from intracellular vesicles to the plasma membrane, in agreement with our previous study using the western blot analysis of GLUT4 translocation in a random-cultured myotube monolayer.[19,20]

In a conventional random-cultured myotube monolayer, it was difficult to match the target myotubes with their GLUT4 translocation activity after the fixation process because it is hard to seek the "contracted target myotubes" on the culture dish during the electrical stimulation. Therefore, the averaged GLUT4 translocation activity of all cultured cells was detected by the western blot analysis, which would underestimate the true activity of the contractile myotubes.

Our device made it possible to easily identify the GLUT4 translocation activity of the contracting myotubes for the first time, by artificially patterning and locally targeted stimulation of the myotubes on the gel sheet. Furthermore, by patterning myotube lines subjected to different stimulation conditions next to each other, high-contrast imaging of the contraction effect on

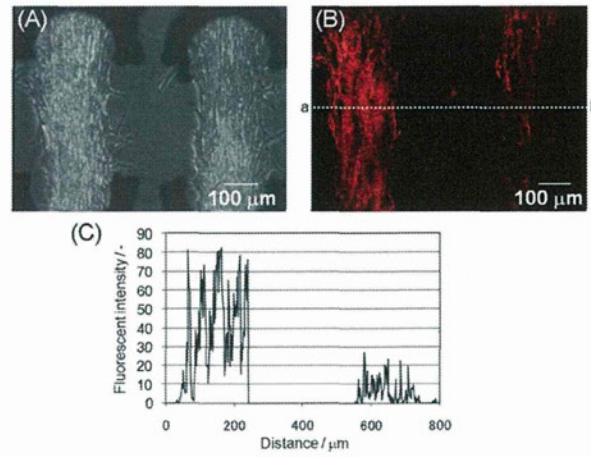

Fig. 6 (A) Phase-contrast micrograph of the transfected myotube line patterns locally stimulated with the PEDOT microelectrode arrays (amplitude, 2 V; duration, 3 ms; frequency, 10 Hz; train, 1 s; interval, 10 s). (B) Fluorescent image of the myotube line patterns immunostained with anti-c-myc first antibody and Alexa Fluor 594-conjugated anti-mouse IgG second antibody. (C) Fluorescent intensity of each immunostained myotube line pattern along the cross-section a–b in (B).

GLUT4 translocation in myotubes was achieved. This device would be applicable for quantitative bioassays of various contraction-induced metabolic alterations in myotubes.

Conclusions

We have developed a micropatterned C_2C_{12} myotubes/fibrin gel culture system integrated with a PEDOT microelectrode array chip for skeletal muscle cell-based bioassay. Arbitrary control of micropatterned myotubes contraction with localized electrical stimulation enabled high-contrast imaging of contraction-induced GLUT4 translocation phenomena in myotubes. This device would easily permit focusing the stimulation site on a desired specific tissue construct, such as a neuromuscular junction formed in a neuron–skeletal muscle cell co-culture. Such applications would be reported in future studies.

Acknowledgements

This work was supported by a Core Research for Evolutional Science and Technology grant from the Japan Science and Technology Agency, partly by Special Coordination Funds for Promoting Science and Technology, Formation of the Innovation Center for Fusion of Advanced Technologies from the Japan Science and Technology Agency, by the Research Grant Program of Asahi Glass Foundation, and by Grants-in-Aid for Scientific Research B (17310080) from the Ministry of Education, Science, and Culture, Japan.

References

1 J. El-Ali, P. K. Sorger and K. F. Jensen, Cells on chips, *Nature*, 2006, **442**, 403–411.
2 H. Aubin, J. W. Nichol, C. B. Hutson, H. Bae, A. L. Sieminski, D. M. Cropek, P. Akhyari and A. Khademhosseini, Directed 3D cell alignment and elongation in microengineered hydrogels, *Biomaterials*, 2010, **31**, 6941–6951.

3 J. T. Lanner, J. D. Bruton, A. Katz and H. Westerblad, Ca^{2+} and insulin-mediated glucose uptake, *Curr. Opin. Pharmacol.*, 2008, **8**, 339–345.

4 S. H. Huang and M. P. Czech, The GLUT4 glucose transporter, *Cell Metab.*, 2007, **5**, 237–252.

5 A. F. M. Johnstone, G. W. Gross, D. G. Weiss, O. H. U. Schroeder, A. Gramowski and T. J. Shafer, Microelectrode arrays: a physiologically based neurotoxicity testing platform for the 21st century, *NeuroToxicology*, 2010, **31**, 331–350.

6 A. Stett, U. Egert, E. Guenther, F. Hofmann, T. Meyer, W. Nisch and H. Haemmerle, Biological application of microelectrode arrays in drug discovery and basic research, *Anal. Bioanal. Chem.*, 2003, **377**, 486–495.

7 N. A. Kotov, J. O. Winter, I. P. Clements, E. Jan, B. P. Timko, S. Campidelli, S. Pathak, A. Mazzatenta, C. M. Lieber, M. Prato, R. V. Bellamkonda, G. A. Silva, N. W. S. Kam, F. Patolsky and L. Ballerini, Nanomaterials for neural interfaces, *Adv. Mater.*, 2009, **21**, 3970–4004.

8 C. E. Schmidt, V. R. Shastri, J. P. Vacanti and R. Langer, Stimulation of neurite outgrowth using an electrically conducting polymer, *Proc. Natl. Acad. Sci. U. S. A.*, 1997, **94**, 8948–8953.

9 C. D. James, R. Davis, M. Meyer, A. Turner, S. Turner, G. Withers, L. Kam, G. Banker, H. Craighead, M. Isaacson, J. Turner and W. Shain, Aligned microcontact printing of micrometer-scale poly-L-lysine structures for controlled growth of cultured neurons on planar microelectrode arrays, *IEEE Trans. Biomed. Eng.*, 2000, **47**, 17–21.

10 W. Cheng, N. Klauke, G. Smith and J. M. Cooper, Microfluidic cell arrays for metabolic monitoring of stimulated cardiomyocytes, *Electrophoresis*, 2010, **31**, 1405–1413.

11 F. Patolsky, B. P. Timko, G. H. Yu, Y. Fang, A. B. Greytak, G. F. Zheng and C. M. Lieber, Detection, stimulation, and inhibition of neuronal signals with high-density nanowire transistor arrays, *Science*, 2006, **313**, 1100–1104.

12 P. Molnar, W. S. Wang, A. Natarajan, J. W. Rumsey and J. J. Hickman, Photolithographic patterning of C_2C_{12} myotubes using vitronectin as growth substrate in serum-free medium, *Biotechnol. Prog.*, 2007, **23**, 265–268.

13 S. T. Cooper, A. L. Maxwell, E. Kizana, M. Ghoddusi, E. C. Hardeman, I. E. Alexander, D. G. Allen and K. N. North, C_2C_{12} co-culture on a fibroblast substratum enables sustained survival of contractile, highly differentiated myotubes with peripheral nuclei and adult fast myosin expression, *Cell Motil. Cytoskeleton*, 2004, **58**, 200–211.

14 T. Cohen-Karni, B. P. Timko, L. E. Weiss and C. M. Lieber, Flexible electrical recording from cells using nanowire transistor arrays, *Proc. Natl. Acad. Sci. U. S. A.*, 2009, **106**, 7309–7313.

15 Y. Haraguchi, T. Shimizu, M. Yamato, A. Kikuchi and T. Okano, Electrical coupling of cardiomyocyte sheets occurs rapidly *via* functional gap junction formation, *Biomaterials*, 2006, **27**, 4765–4774.

16 H. Fujita, K. Shimizu and E. Nagamori, Application of a cell sheet-polymer film complex with temperature sensitivity for increased mechanical strength and cell alignment capability, *Biotechnol. Bioeng.*, 2009, **103**, 370–377.

17 K. Nagamine, T. Kawashima, T. Ishibashi, H. Kaji, M. Kanzaki and M. Nishizawa, Micropatterning contractile C_2C_{12} myotubes embedded in a fibrin gel, *Biotechnol. Bioeng.*, 2010, **105**, 1161–1167.

18 M. Nishizawa, H. Nozaki, H. Kaji, T. Kitazume, N. Kobayashi, T. Ishibashi and T. Abe, Electrodeposition of anchored polypyrrole film on microelectrodes and stimulation of cultured cardiac myocytes, *Biomaterials*, 2007, **28**, 1480–1485.

19 T. Nedachi and M. Kanzaki, Regulation of glucose transporters by insulin and extracellular glucose in C_2C_{12} myotubes, *Am. J. Physiol.: Endocrinol. Metab.*, 2006, **291**, E817–E828.

20 T. Nedachi, H. Fujita and M. Kanzaki, Contractile C_2C_{12} myotube model for studying exercise-inducible responses in skeletal muscle, *Am. J. Physiol.: Endocrinol. Metab.*, 2008, **295**, E1191–E1204.

21 S. Mitsushima, S. Kawahara, K. I. Ota and N. Kamiya, Consumption rate of Pt under potential cycling, *J. Electrochem. Soc.*, 2007, **154**, B153–B158.

22 T. S. Hansen, K. West, O. Hassager and N. B. Larsen, Direct fast patterning of conductive polymers using agarose stamping, *Adv. Mater.*, 2007, **19**, 3261–3265.

ACS Macro Letters

Letter

pubs.acs.org/macroletters

Conducting Polymer Microelectrodes Anchored to Hydrogel Films

Yuichiro Ido,[†] Daisuke Takahashi,[†] Masato Sasaki,[†] Kuniaki Nagamine,[†,‡] Takeo Miyake,[†,‡] Piotr Jasinski,[§] and Matsuhiko Nishizawa*[,†,‡]

[†]Department of Bioengineering and Robotics, Graduate School of Engineering, Tohoku University, 6-6-01 Aramaki, Aoba-ku, Sendai 980-8579, Japan

[‡]JST-CREST, Sanbancho, Chiyoda-ku, Tokyo 102-0075, Japan

[§]Faculty of Electronics, Telecommunication and Informatics, Gdansk University of Technology, ul. Narutowicza 11/12, 80-233 Gdansk, Poland

Supporting Information

ABSTRACT: We report the fabrication of totally organic hydrogel-based microelectrodes of poly(3,4-ethylenedioxythiophene) (PEDOT), which exhibit a lowered sheet resistivity of about 100 Ω/□. The preparation process starts with the electrodeposition of conductive PEDOT (ca. 20 S cm^{-1}) on Pt microelectrodes. After laminating hydrogels onto the PEDOT-modified Pt electrode substrates, a second PEDOT (low conductivity) layer was electrodeposited to anchor the first PEDOT film to the hydrogel. Finally, the hydrogel sheet with PEDOT micropatterns was peeled off by taking advantage of the electroactuation property of PEDOT. The process proved to be versatile, allowing the use of most natural and synthetic hydrogels including agarose, collagen, polyacrylamide, and so on.

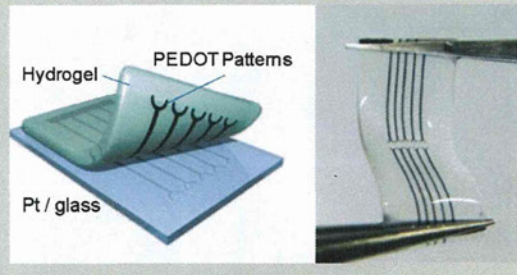

Conducting polymers (CPs) such as poly(3,4-ethylenedioxythiophene) (PEDOT) are attractive electrode-coating materials, having the advantages of biocompatibility and low electrical impedance.[1−3] They have been utilized for implanted electronics[4−6] and in vitro devices for culturing cells.[7−11] In contrast to these conventional metal-supported CP electrodes, we have attempted to prepare an autonomous CP microelectrode on a hydrogel substrate that contains ~80% H_2O in order to develop a totally organic, flexible, and molecularly permeable electrode. All of the existing printing methods using screens, inkjet systems, or microstamps, require the drying of fluid inks and, thus, cannot be used for printing on a moist gel substrate. Recently, we found that the electrodeposition of PEDOT into an agarose film produces such a gel-based electrode, which is soft enough to contract synchronously with the motion of muscle cells.[12] However, the sheet resistivity of that PEDOT electrodes formed in the agarose (ca. 10 kΩ/□) was unfortunately higher than expected.[13] Apparently, dendritic growth through the hydrogel matrix[5] resulted in a larger surface area (manifested by a larger double layer capacitance) but a lower electrical conductivity due to the sparse structure. An improvement in the conductive property of the PEDOT/hydrogel electrodes should expand their possible applications.

We report herein an improved process to prepare more conductive PEDOT micropatterns on hydrogels. As shown in Figure 1a, the dense PEDOT film was first electropolymerized on Pt microelectrodes. Owing to the absence of hydrogel, we can freely employ appropriate polymerization conditions. For example, the use of CH_3CN as solvent leads to highly conductive PEDOT, as described later; the polymerization from aqueous EDOT solutions would have advantages for the biofunctionalization of PEDOT such as enzyme immobilization.[3,14] Next, as illustrated in Figure 1b,c, after forming agarose or laminating a precured other hydrogel onto the PEDOT-modified electrode substrates, a second PEDOT layer was electropolymerized from aqueous EDOT solution to anchor the first conductive PEDOT film to the hydrogel matrix. The process we previously reported[12] depended only on this sparse PEDOT for electrode preparation. Finally, the hydrogel film with PEDOT micropatterns was peeled from the Pt electrode substrate (Figure 1d) by taking advantage of the electrochemical elastic actuation of PEDOT (±0.5 V vs Ag/AgCl).[15,16]

Figure 2 shows photographs of typical specimens after the peeling process with different polymerization charges of the second PEDOT, proving its importance for nondisruptive peeling. The 1 × 1 cm Pt electrodes on glass substrates were first coated with a 300 mC PEDOT film. Next, a melted 2.8 wt % agarose solution was poured over the substrate and gelated by cooling in room temperature (2 mm thickness). Then a second PEDOT layer was electropolymerized at charges of (a) 0, (b) 100, and (c) 200 mC. Finally, twin cycles of electrochemical elastic actuation was applied for inducing stress at the polymer/electrode interface, leading to eventually

Received: December 22, 2011
Accepted: February 24, 2012
Published: February 28, 2012

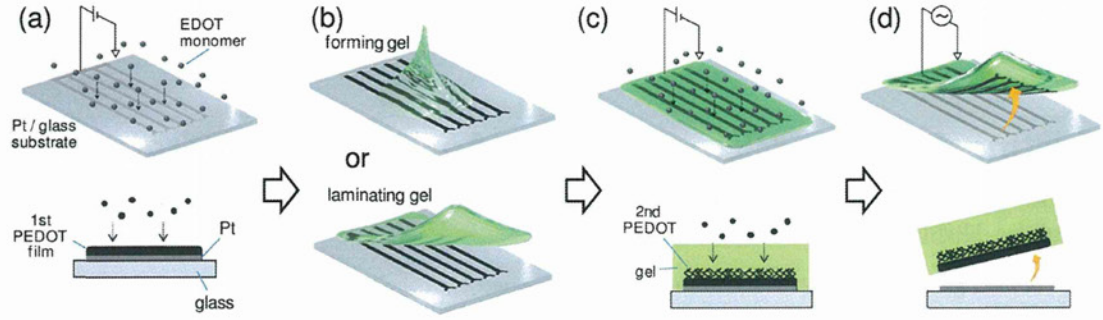

Figure 1. Schematic illustrations of the fabrication process for a conducting polymer/hydrogel electrode: (a) PEDOT was electropolymerized on a Pt microelectrode substrate; (b) a hydrogel sheet was formed or laminated on the substrate; (c) PEDOT was again polymerized; (d) then a PEDOT/hydrogel electrode was peeled from the substrate after electrochemical elastic actuation.

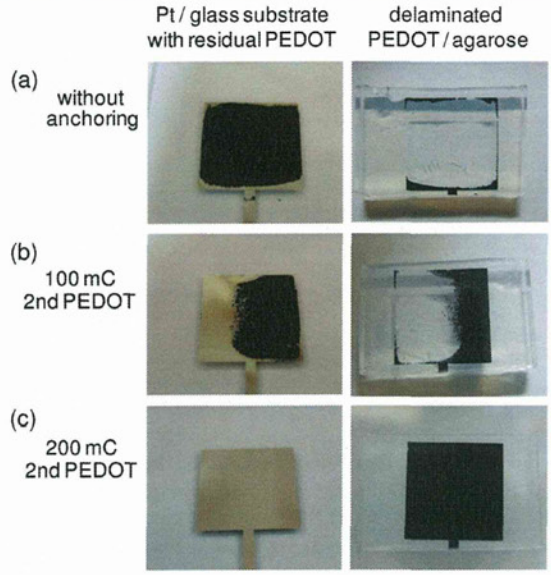

Figure 2. Photographs of Pt/glass substrates and agarose sheets after the peeling process with twin redox cycles (±0.5 V vs Ag/AgCl). The polymerization charge of the first PEDOT films was 300 mC and (a) 0, (b) 100, and (c) 200 mC for the second PEDOT layers. The polymerization was potentiostatic at 1.0 V vs Ag/AgCl in 0.1 M $LiClO_4$ aqueous solution of EDOT.

detachment. In the case without the second PEDOT deposition, a clean transfer of the pattern has never achieved (Figure 2a). The second PEDOT of 100 mC resulted in an irregular, partial transfer (Figure 2b). On the other hand, the second PEDOT of 200 mC ensured 100% transfer every time (Figure 2c), indicating that a sufficient amount of a second dendritic PEDOT layer (more than 200 mC) can serve as an effective anchor to connect the first PEDOT film and the hydrogel matrix. It is worth noting that a prior hydrophilic modification of the glass substrates with aminosilane is also necessary for nondisruptive peeling; we immersed Pt/glass substrates in 20 mM 3-aminopropyltriethoxysilane/heptane for 6 h for forming the self-assembling monolayer of aminosilane on the surface of the glass part of the substrates. Without these treatments, the naturally impure glass surface often causes anisotropic lateral growth of the polymer from the Pt electrode along the surface of the surrounding glass, resulting in adhesion between the CP and the glass substrate.[11]

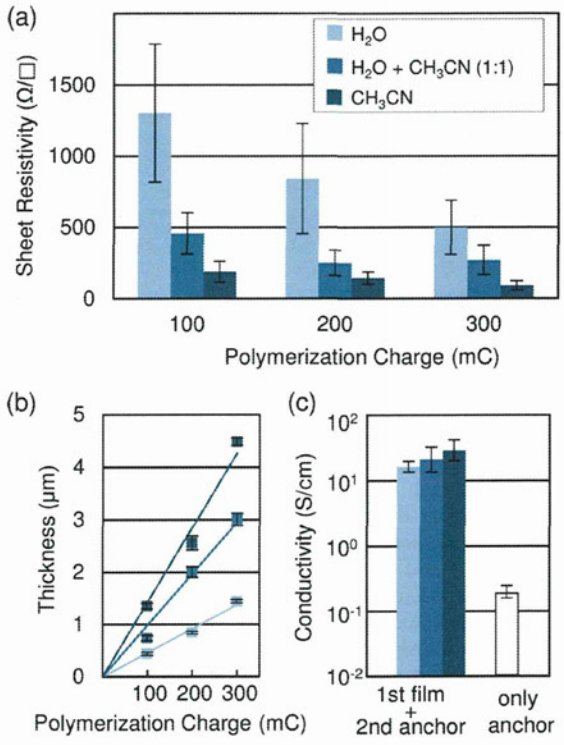

Figure 3. (a) Sheet resistivity of the PEDOT patterns (1 × 1 cm) transferred to agarose films as functions of polymerization charge of the first PEDOT film (100, 200, and 300 mC) and the solvents used for the polymerization (H_2O, CH_3CN, and their 1:1 mixture). The mean values (±standard deviation) of at least three independent specimens are given. The polymerization was potentiostatic at 1.0 V in each solution containing 50 mM EDOT and 0.1 M $LiClO_4$. The charge for second PEDOT layer was 300 mC. (b) Thickness of the first PEDOT films measured by a surface texture analyzer (DEKTAC 150). (c) Conductivity of the PEDOTs calculated by using their thickness. The conductivity value in the case without the first PEDOT film (only the second PEDOT anchor) is also shown.

With the polymerization charge of the second PEDOT fixed at 300 mC, we studied next the sheet resistivity of the peeled PEDOT patterns by changing the polymerization conditions of the first PEDOT films. The resistivity measurements were conducted under wet conditions by the two-point probe method around 0.4 V versus Ag/AgCl, where the PEDOT is in

dx.doi.org/10.1021/mz2002406 | ACS Macro Lett. 2012, 1, 400–403

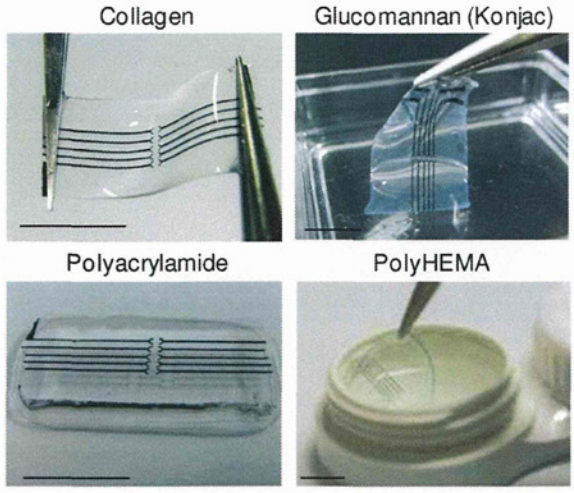

Figure 4. Photographs of the PEDOT microelectrodes anchored to the preliminarily molded hydrogel films of collagen (0.3 mm thick), glucomannan (1 mm thick), polyacrylamide (1 mm thick), and a commercial soft contact lens made of poly(2-hydroxyethyl methacrylate). Scale bar: 5 mm.

the oxidized form. The ohmic property was checked by varying the bias between the probes. Figure 3a shows that increasing the polymerization charge up to 300 mC decreased the sheet resistivity to less than 500 Ω/□, a value 2 orders of magnitude lower than that (ca. 10 kΩ/□) of the PEDOT electrode prepared by our previous process without the first PEDOT film.[12] In particular, the PEDOT film prepared using CH_3CN solvent showed the lowest resistivity, about 100 Ω/□. Presumably, polymerization at greater than 300 mC will further decrease the sheet resistivity. As shown in Figure 3b, the thickness of the first PEDOT film, measured by a surface texture analyzer, were found vary with solvents used, probably due to difference in the Coulombic efficiency of electrodeposition. The 300 mC/cm^2 polymerization led to a thickness of about 1.5 μm in H_2O, 3.0 μm in H_2O/CH_3CN, and 4.5 μm in CH_3CN, respectively. Figure 3c depicts the conductivity of the transferred PEDOTs calculated taking account of their thickness. The conductivity values of the present PEDOT electrodes reach the range of 10^1 S/cm, regardless of the kind of solvent, the value being comparable to the generally known conductivity of the PEDOT.[13] For reference, the second PEDOT layer grown in agarose showed a thickness of about 5 μm for 300 mC/cm^2,[12] as also judged from the cross section (Supporting Information, Figure S1). Because the conductivity of the second PEDOT layer grown in agarose was in the range of 10^{-1} S/cm, its contribution to the net conductivity is small; it functions simply as an anchor between the first PEDOT film and the hydrogel.

The process used to prepare PEDOT micropatterns was versatile, being also successful with precured films of other kinds of natural hydrogels (collagen, glucomannan) and synthetic hydrogels (polyacrylamide, poly(2-hydroxyethyl methacrylate)), as shown in Figure 4. In addition, the PEDOT patterning process is adaptive to the variations of elasticity, thickness and shapes of the hydrogels. For example, even a commercial soft contact lens can be used as the substrate for PEDOT electrodes. Although the structural and electrical characters of the second PEDOT would be somewhat different by the hydrogels used, they functioned well as the anchor for nondisruptive peeling of the first PEDOT, as with the case of agarose. Among the hydrogels we studied, only the fibrin gel could not be used as the substrate for PEDOT electrodes. The electrostatic and chemical conditions in fibrin may inhibit the polymerization of the second PEDOT.

The hydrogel-based CP micropatterns discussed here represent a totally organic, moist, flexible, and molecularly permeable electrode that can be combined with cells and tissues without disturbing the physiological conditions including the continuous supply of O_2 and nutrients. Such properties are ideal for use as in vivo and in vitro electrodes for stimulation and recording. Besides such cellular applications, these improved conductivity CP/gel electrodes should be applicable to a variety of hydrogel-based electronic systems such as iontophoretic drug delivery.

■ ASSOCIATED CONTENT

Supporting Information

The optical microscope image of the cross section of PEDOT/agarose electrode. This material is available free of charge via the Internet at http://pubs.acs.org.

■ AUTHOR INFORMATION

Corresponding Author

*E-mail: nishizawa@biomems.mech.tohoku.ac.jp.

Notes

The authors declare no competing financial interest.

■ ACKNOWLEDGMENTS

The authors thank BEX Co. for the kind donation of collagen sheets. This work was partly supported by The Research Grant Program of Asahi Glass Foundation and by Grants-in-Aid for Scientific Research B (No. 17310080) from the Ministry of Education, Science, and Culture, Japan.

■ REFERENCES

(1) Skotheim, T., Reynolds, J. R., Eds. *Handbook of Conducting Polymers*; Marcel Dekker: New York, 2006.
(2) Leger, J., Berggren, M.; Carter, S., Eds. *Iontronics*; CRC Press: New York, 2011.
(3) Guiseppi-Elie, A. *Biomaterials* **2010**, *31*, 2701−2716.
(4) Kim, D.-H.; Wiler, J. A.; Anderson, D. J.; Kipke, D. R.; Martin, D. C. *Acta Biomater.* **2010**, *6*, 57−62.
(5) Kim, D.-H.; Abidian, M.; Martin, D. C. *J. Biomed. Mater. Res., Part A* **2004**, *71A*, 577−585.
(6) George, P. M.; Lyckman, A. W.; LaVan, D. A.; Hegde, A.; Leung, Y.; Avasare, R.; Testa, C.; Alexander, P. M.; Langer, R.; Sur, M. *Biomaterials* **2005**, *26*, 3511−3519.
(7) Schmidt, C; Shastri, V. R.; Vacanti, J. P.; Langer, R. *Proc. Natl. Acad. Sci. U.S.A.* **1997**, *94*, 8948−8953.
(8) Kim, S. Y.; Kim, K.-M.; Hoffman-Kim, D.; Song, H.-K.; Palmore, G. T. R. *ACS Appl. Mater. Interface* **2010**, *3*, 16−21.
(9) Svennersten, K.; Bolin, M. H.; Jager, E. W. H.; Berggren, M.; Richter-Dahlfors, A. *Biomaterials* **2009**, *30*, 6257−6264.
(10) Nyberg, T.; Shimada, A.; Torimitsu, K. *J. Neurosci. Methods* **2007**, *160*, 16−25.
(11) Nishizawa, M.; Nozaki, H.; Kaji, H.; Kitazume, T.; Kobayashi, N.; Ishibashi, T.; Abe, T. *Biomaterials* **2007**, *28*, 1480−1485.
(12) Sekine, S.; Ido, Y.; Miyake, T.; Nagamine, K.; Nishizawa, M. *J. Am. Chem. Soc.* **2010**, *132*, 13174−13175.
(13) Groenendaal, L. B.; Jonas, F.; Freitag, D.; Pielartzik, H.; Reynolds, J. R. *Adv. Mater.* **2000**, *12*, 481−494.
(14) Gerard, M.; Chaubey, A.; Malhotra, B. D. *Biosens. Bioelectron.* **2002**, *17*, 345−359.

(15) Jager, E. W. H.; Smela, E.; Inganas, O. *Science* **2000**, *290*, 1540–1545.
(16) Han, G.; Shi, G. *Sens. Actuators, B* **2006**, *113*, 259–264.

Electrochimica Acta 82 (2012) 175–178

Contents lists available at SciVerse ScienceDirect

Electrochimica Acta

journal homepage: www.elsevier.com/locate/electacta

Sheet-shaped biofuel cell constructed from enzyme-modified nanoengineered carbon fabric

Keigo Haneda[a], Syuhei Yoshino[a], Takuya Ofuji[a], Takeo Miyake[a,b,*], Matsuhiko Nishizawa[a,b,*]

[a] Department of Bioengineering and Robotics, Tohoku University, 6-6-1 Aramaki Aoba, Aoba-ku, Sendai 980-8579, Japan
[b] Core Research for Evolutional Science and Technology (CREST), Japan Science and Technology Agency, Tokyo 102-0075, Japan

ARTICLE INFO

Article history:
Received 27 November 2011
Received in revised form 7 January 2012
Accepted 9 January 2012
Available online 14 February 2012

Keywords:
Biofuel cell
Carbon fabric
Carbon nanotube
Gas-diffusion cathode

ABSTRACT

A strip of carbon fabric (CF) electrode modified with multiwalled carbon nanotubes and subsequently fructose dehydrogenase (FDH) showed an oxidation current density of ~11 mA cm^{-2} in stirred 200 mM fructose solution. Obtaining a sufficient dispersion of the nanotubes during its modification was found to be critical to ensure such a performance of the FDH anode. For use with this anode, a CF strip modified with ketjenblack (KB) and bilirubin oxidase (BOD) served as a gas-diffusion cathode for the reduction of O_2 from air at a current density of ~2 mA cm^{-2}. The FDH-modified CF strip and the BOD-modified CF strip were stacked with an agarose film that retained an electrolyte solution and fuel (fructose) to construct a totally flexible sheet-shaped biofuel cell. This assembly allowed bending of 44° without affecting the maximum output power density, 550 μW cm^{-2} obtained at 0.4 V.

1. Introduction

Enzyme-based biofuel cells that generate electricity through enzymatic oxidation of biological fuels like sugars and alcohols have attracted attention as ubiquitous, safe power sources [1–23]. Recent rapid improvements in their power performance up to mW cm^{-2} levels by employing nanostructured carbon electrodes [24–28] have motivated various applications including a sheet-shaped cell that can be combined with advanced flexible film electronics [29,30]. However, the brittle carbon electrodes, which are generally aggregates of particulate or tubular nanocarbons, often limit the design and uses of such biofuel cells.

In the present work, we have prepared a totally flexible, sheet-shaped biofuel cell by using a carbon fabric (CF) as the flexible, conductive base for the enzyme electrodes. We modified the CF strip with multiwalled carbon nanotubes (CNTs) and fructose dehydrogenase (FDH) for the oxidation of fructose, and with ketjenblack (KB) and bilirubin oxidase (BOD) for the reduction of oxygen in the ambient air. Both FDH and BOD are capable of efficient "direct electron transfer" with common electrode materials including carbon [10,16,21,31,32]. The pre-modifications with CNT or KB increase the specific surface area of the CF electrodes, resulting in effective enzyme immobilization and, ultimately, higher power. The FDH anode strip and the BOD cathode strip are stacked with a hydrogel film that retains the electrolyte solution and fuel (fructose), as shown in Fig. 1. This assembly provides a stand-alone, sheet-shaped power source that can be bent without loss of output power.

2. Experimental

2.1. Preparation of carbon fabric anode

A 5 mm × 5 mm strip of carbon fabric (CF) (TCC-3250, donated from Toho Tenax Co.) was first modified with multiwalled carbon nanotubes (Baytubes, donated from Bayer Material Science Co.) to increase the specific surface area. The carbon nanotubes (CNTs) were pretreated by heating at 400 °C for 11 h and by immersing in mixed acid ($H_2SO_4 + HNO_3$ in a 1:3 ratio) for 5 h. The treated CNT were dispersed in water containing Triton X-100 surfactant (0.05, 0.1, 0.5 or 1%). A 40 μl aliquot of the 10 mg ml^{-1} CNT dispersion was dropped on a CF strip (0.32 mm thickness, 0.25 cm^2 geometric area) and dried in air, followed by thoroughly washing out the surfactant by soaking in a pure McIlvaine buffer solution for more than 1 h with stirring. Then, the CNT-modified CF strip was immersed in a 5 mg ml^{-1} solution of D-fructose dehydrogenase (FDH) (EC1.1.99.11, 169.9 U mg^{-1}, ca. 140 kDa, from Gluconobacter, purchased from Toyobo Enzyme Co.) for FDH immobilization [28]. It has been reported that FDH works as a electrocatalyst for oxidation of fructose without electron transfer mediators [10,16,21,31]. The flavin-containing subunit of FDH accepts electrons from fructose, and transfers these electrons to the heme C-containing subunit that can electrically communicate with electrode [31].

* Corresponding authors at: Department of Bioengineering and Robotics, Tohoku University, 6-6-1 Aramaki Aoba, Aoba-ku, Sendai 980-8579, Japan.
Tel.: +81 22 795 7003; fax: +81 22 795 7003.
E-mail address: nishizawa@biomems.mech.tohoku.ac.jp (M. Nishizawa).

0013-4686/$ – see front matter © 2012 Published by Elsevier Ltd.
doi:10.1016/j.electacta.2012.01.112

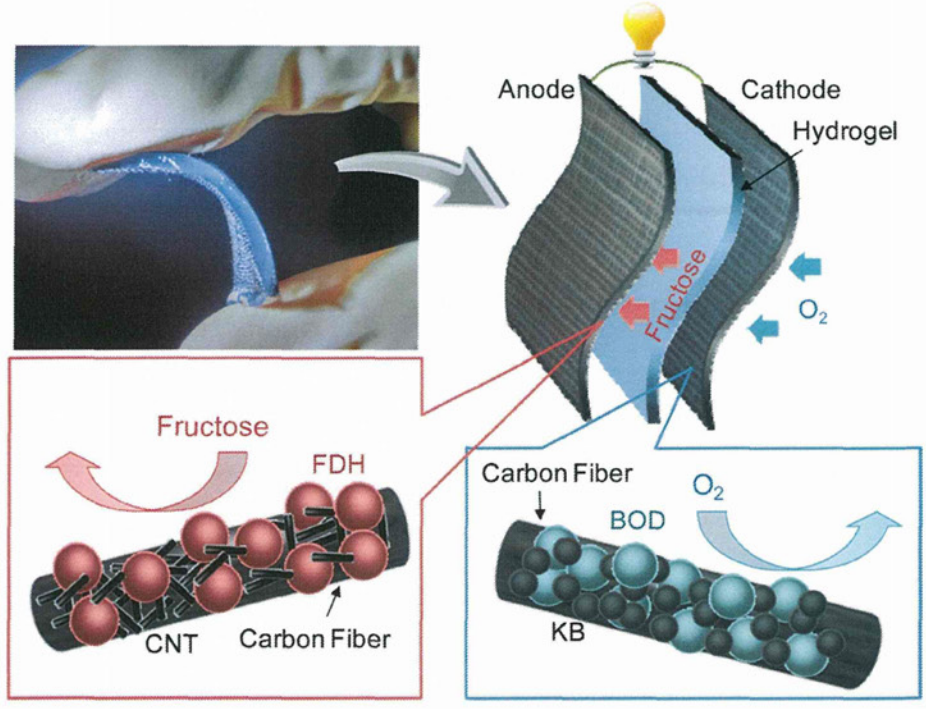

Fig. 1. A sheet-shaped biofuel cell constructed by stacking enzyme-modified nanoengineered carbon fabric strips with a hydrogel film that retains electrolyte solutions and fructose fuel.

2.2. Preparation of gas-diffusion carbon fabric cathode

The preparation of the cathode basically followed the procedures used for our previous carbon paper-based BOD cathode [23]. BOD is one of multi-cupper oxidases that can directly catalyze four-electron reduction of O_2 to H_2O even without electron transfer mediators [10,16,32]. A 25 μl aliquot of a 8 mg ml^{-1} solution of ketjenblack (KB)/poly(tetrafluoroethylene) (PTFE) (1: 1) was put on a CF strip and dried in air. The surface of the KB-modified CF electrode was further modified with a 0.1 ml solution of 5 mg ml^{-1} bilirubin oxidase (BOD, EC 1.3.3.5, 2.5 U/mg, from *Myrothecium*). After drying in air, the strip was additionally coated with the KB solution to make surface hydrophobic. The geometric size was the same as the anode (0.32 mm thickness, 0.25 cm^2 area).

2.3. Electrochemical measurements

The performance of the CF electrodes was analyzed by a three-electrode system (BSA, 730C electrochemical analyzer) in solution using a Ag/AgCl reference and a platinum counter electrode. The FDH-modified anodes were evaluated in stirred McIlvaine buffer (pH 5.0) containing 200 mM fructose, while the BOD-modified cathodes were in air-saturated McIlvaine buffer (pH 5.0). The performance of a biofuel cell constructed with the FDH-modified CF anode, the BOD-modified CF cathode, and the fructose-containing agarose film (3 mm thick) was evaluated from the cell voltage upon connecting with a variable external resistance between 180 Ω and 10 kΩ. For preparing the fructose-containing agarose films, a 150 mM McIlvaine buffer containing 200 mM fructose was first warmed to dissolve 1.5 wt% agarose, and molded with cooling. The current and the power were derived from the detected cell voltage and the resistance. Unless otherwise indicated, the electrochemical measurements were carried out at room temperature, around 25 °C.

3. Results and discussion

3.1. Performance of FDH/CNT/CF bioanodes

Fig. 2 shows cyclic voltammograms of the FDH/CNT/CF electrodes (solid plots) at 10 mV s^{-1} in a stirred buffer solution containing 200 mM fructose. In comparison with the FDH/CF electrode prepared without CNTs (broken line plot), the increased specific surface area produced by CNT-modification obviously increased the current density by at least an order of magnitude. In fact, the measured double-layer capacitance of the CNT-modified electrodes has a 2 orders larger value (ca. 6.5 mF cm^{-2}) than that of the original CF (0.07 mF cm^{-2}). Importantly, the oxidation current

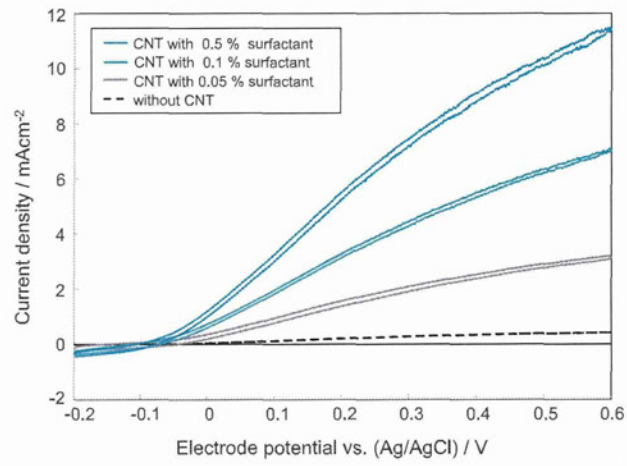

Fig. 2. Cyclic voltammograms of FDH-immobilized CF strip electrodes at 10 mV s^{-1} in a stirred buffer solution (pH 5) containing 200 mM fructose. The CF electrodes were pre-modified with CNTs dispersed with different concentrations of Triton X-100 surfactant.

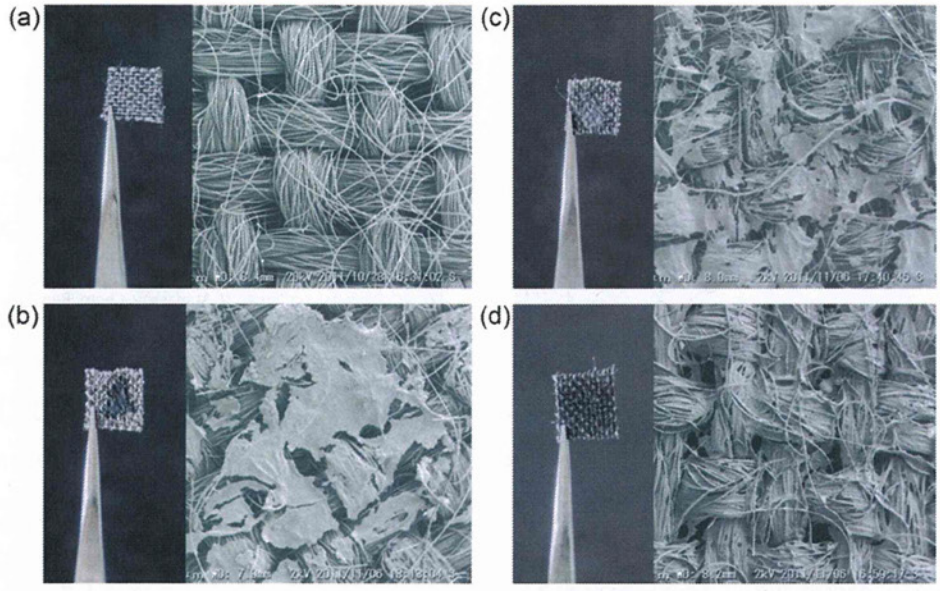

Fig. 3. Photographs and SEM images of (a) a bare CF strip and (b–d) CNT-modified strips. The CNT dispersions were prepared with (b) 0.05%, (c) 0.1%, (d) 0.5% Triton X-100 surfactant.

density depended on the concentration of the Triton X-100 surfactant used for the CNT dispersion (0.05, 0.1 and 0.5%), despite the fact that all these CNT-modified electrodes had similar capacitance (similar specific surface area). The use of 1% surfactant brought no significant further change over that from 0.5% surfactant. Fig. 3 shows the surface structure of the CNT-adsorbed CF strips observed by optical and scanning electron microscopies. The CNT dispersions with 0.05% and 0.1% surfactant are found to precipitate on the CF surface (Fig. 3b and c). In contrast, the CNT dispersion with 0.5% surfactant seems to entirely penetrate into the CF strip. This uniform modification with CNT would be a main reason of the enhanced anode performance, up to a value of 11.5 mA cm^{-2} at 0.6 V.

3.2. Performance of gas-diffusion biocathodes

Fig. 4 shows cyclic voltammograms of a BOD-modified CF cathode at 10 mV s^{-1}. The electrode strip was put on an oxygenic pH 5.0 buffer solution so as to contact the solution by the BOD-modified face (purple solid plot). The reduction current density reaches ~0.76 mA cm^{-2} (at 0 V), which is 1.5 times larger than that measured by the biocathode immersed into the solution (broken line plot). This increase of current density is a result of a better oxygen supply from the ambient air through the CF. Moreover, an additional KB coating onto the BOD-modified face of the CF strip enhanced the performance further to 2.0 mA cm^{-2}, which was reproducible within 10% variation (1.8–2.2 mA cm^{-2}) for four independent electrode specimens. Presumably, the hydrophobic nature of that coating controls excess penetration of solution into the CF electrodes [23]. The reduction current density at 0 V varied 1.8–2.2 mA cm^{-2}.

3.3. Performance of the flexible biofuel cell

A biofuel cell was constructed with the FDH/CNT-modified CF anode and the KB/BOD/KB-modified gas-diffusion CF cathode. These electrodes were attached to both sides of an agarose hydrogel (3 mm thick) made with 150 mM McIlvaine buffer solution (pH 5.0) containing 200 mM fructose. The enzyme-modified hydrophilic anode appeared to become moistened by blotting of the solution from the hydrogel layer. On the other hand, the O_2 reduction at the hydrophobic cathode proceeded at the three-phase boundary of the hydrogel–electrode interface. Fig. 5 shows typical examples of the cell performance. The open-circuit voltage of the cell was 0.7 V, which is similar to the difference between the potentials at which fructose oxidation and oxygen reduction start to occur in cyclic voltammograms (−0.1 V in Fig. 2 and 0.6 V in Fig. 4, respectively). The maximum values of current and power densities are determined by the BOD-cathode because of its comparatively lower performance than FDH-anode. Even as a stand-alone assembly with the fuel (fructose)-containing gel sheet, the maximum power density reached 550 μW cm^{-2} at 0.4 V. Importantly, this device could be repeatedly bent to a 44° angle without significant loss of output power. Bending in excess of this value caused fracture of the agarose hydrogel sheet; our device can be made more resistant to mechanical stress by using more elastic hydrogels such as polyvinylalcohol.

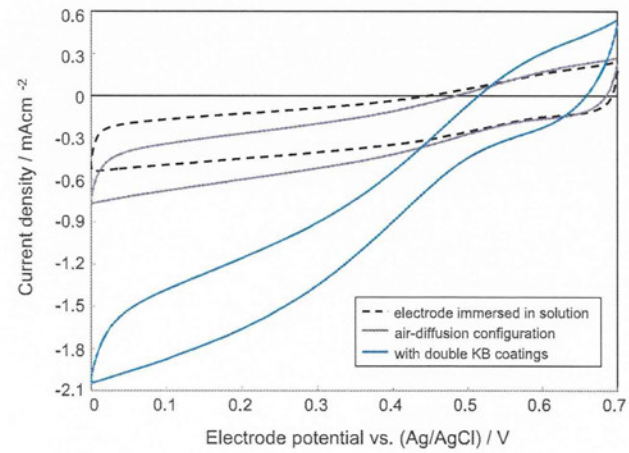

Fig. 4. Cyclic voltammograms of O_2 reduction at a BOD/KB-modified CF strip measured at 10 mV s^{-1} in the solution (broken line) and on the solution (air-diffusion configuration, solid lines). The activity of the CF electrode was enhanced by further modification with KB after the BOD immobilization.

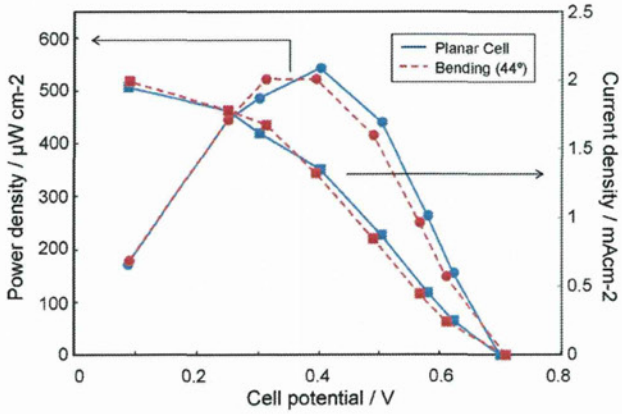

Fig. 5. Performance of the sheet-shaped biofuel cell (1 cm × 0.2 cm) with and without bending. The internal agarose layer was made with 150 mM McIlvaine buffer solution (pH 5.0) containing 200 mM fructose.

4. Conclusions

We have developed a totally flexible, sheet-shaped biofuel cell device by stacking a FDH/CNT-modified CF strip, a KB/BOD/KB-modified gas-diffusion CF strip, and an agarose hydrogel film that retains electrolyte solution and fuel (fructose). The results presented include two strategies to improve the performance of the device. (1) A CF anode modified with an appropriate CNT dispersion showed higher activity. (2) The gas-diffusion biocathode was improved by optimizing its hydrophobicity. The improved biofuel cell sheet produced a maximum power density of 550 $\mu W\,cm^{-2}$ at 0.4 V even when bent. Such a flexible, sheet-shaped power source could be combined in the future with flexible electronic to make wearable devices.

Acknowledgements

The authors thank Dr. Piotr Jasinski, Gdansk University of Technology, for his helpful advice. The carbon fabric and carbon nanotubes were kindly donated from Toho Tenax Co. and Bayer Co., respectively. This work was partly supported by the Noguchi Institute.

References

[1] I. Willner, E. Katz, Bioelectronics, Wiley-VCH, Weinheim, 2005.
[2] G.T.R. Palmore, H. Bertschy, S.H. Bergens, G.M. Whitesides, J. Electroanal. Chem. 443 (1998) 155.
[3] I. Willner, Y.M. Yan, B. Willner, R. Tel-Vered, Fuel Cell. 1 (2009) 7.
[4] M.J. Moehlenbrock, S.D. Minteer, Chem. Soc. Rev. 37 (2008) 1188.
[5] W. Gellett, M. Kesmez, J. Schumacher, N. Akers, S.D. Minteer, Electroanalysis 22 (2010) 727.
[6] A. Heller, B. Feldman, Chem. Rev. 108 (2008) 2482.
[7] S.C. Barton, J. Gallaway, P. Atanassov, Chem. Rev. 104 (2004) 4867.
[8] J.A. Cracknell, K.A. Vincent, F.A. Armstrong, Chem. Rev. 108 (2008) 2439.
[9] J. Wang, Talanta 75 (2008) 636.
[10] M.J. Cooney, V. Svoboda, C. Lau, G. Martin, S.D. Minteer, Energy Environ. Sci. 1 (2008) 320.
[11] S.A. Neto, J.C. Forti, A.R. De Andrade, Electrocatalysis 1 (2010) 87.
[12] I. Ivanov, T. Vidakovic-Koch, K. Sundmacher, Energies 3 (2010) 803.
[13] Yu E. Hao, K. Scott, Energies 3 (2010) 23.
[14] S. Rubenwolf, S. Kerzenmacher, R. Zengerle, F.V. Stetten, Appl. Microbiol. Biotechnol. 89 (2011) 1315.
[15] M.H. Osman, A.A. Shah, F.C. Walsh, Biosens. Bioelectron. 26 (2011) 3087.
[16] Y. Kamitaka, S. Tsujimura, N. Setoyama, T. Kajino, K. Kano, Physiol. Chem. Phys. 9 (2007) 1793.
[17] R.A. Bullen, T.C. Arnot, J.B. Lakeman, F.C. Walsh, Biosens. Bioelectron. 21 (2006) 2015.
[18] J. Kim, H. Jia, P. Wang, Biotechnol. Adv. 24 (2006) 296.
[19] J. Wang, Y. Lin, Trends Anal. Chem. 27 (2008) 619.
[20] E. Katz, I. Willner, Chem. Phys. Chem. 5 (2004) 1084.
[21] L. Gorton, A. Lindgren, T. Larsson, F.D. Munteanu, T. Ruzgas, I. Gazaryan, Anal. Chim. Acta 400 (1999) 91.
[22] T. Miyake, M. Oike, S. Yoshino, Y. Yatagawa, K. Haneda, M. Nishizawa, Lab Chip 10 (2010) 2574.
[23] T. Miyake, K. Haneda, N. Nagai, Y. Yatagawa, H. Onami, S. Yoshino, T. Abe, M. Nishizawa, Energy Environ. Sci. 4 (2011) 5008.
[24] F. Gao, L. Viry, M. Maugey, P. Poulin, N. Mano, Nat. Commun. 1 (2010) 2.
[25] H. Sakai, T. Nakagawa, Y. Tokita, T. Hatazawa, T. Ikeda, S. Tsujimura, K. Kano, Energy Environ. Sci. 2 (2009) 133.
[26] S. Tsujimura, A. Nishina, Y. Hamano, K. Kano, S. Shiraishi, Electrochem. Commun. 12 (2010) 446.
[27] A. Zebda, C. Gondran, A.L. Goff, M. Holzinger, P. Cinquin, S. Cosnier, Nat. Commun. 2 (2011) 370.
[28] T. Miyake, S. Yoshino, T. Yamada, K. Hata, M. Nishizawa, J. Am. Chem. Soc. 133 (2011) 5129.
[29] H. Nishide, K. Oyaizu, Science 319 (2008) 737.
[30] J.A. Rogers, T. Someya, Y. Huang, Science 327 (2010) 1603.
[31] M. Tominaga, C. Shirakihara, I. Taniguchi, J. Electroanal. Chem. 610 (2007) 1.
[32] S. Shleev, J. Tkac, A. Christenson, T. Ruzgas, A.I. Yaropolov, J.M. Whittaker, L. Gorton, Biosens. Bioelectron. 20 (2005) 2517.